Eur. Phys. J. Plus (2021) 136:818
https://doi.org/10.1140/epjp/s13360-021-01761-w

THE EUROPEAN PHYSICAL JOURNAL PLUS

Regular Article

Poroelasticity framework for stress/strain responses of the multi-phase circular/annular systems resting on various types of elastic foundations

Hu Zhao[1,a], **Linghui Wang**[2,b], **Alibek Issakhov**[3,4,c], **Hamed Safarpour**[5,d]

[1] Sichuan Highway Planning Survey Design and Research Institute Ltd., Chengdu 610000, Sichuan, China
[2] Exploration and Production Research Institute, Sinopec Southwest Oil & Gas Company, Chengdu 610041, Sichuan, China
[3] Al-Farabi Kazakh National University, Almaty, Kazakhstan
[4] Kazakh-British Technical University, Almaty, Kazakhstan
[5] Department of Mechanics, Imam Khomeini International University, Qazvin, Iran

Received: 9 September 2020 / Accepted: 16 July 2021

Abstract This paper investigates bending responses of three-phase multi-scale hybrid laminated nanocomposite reinforced axisymmetric circular/annular plates based upon the three-dimensional poroelasticity theory for various sets of boundary conditions. The two-parameter elastic foundation (Pasternak type) is developed by taking into account the torsional interaction. Using compatibility conditions, the sandwich structure with two, three, five, and seven layers is modeled. The state-space-based differential quadrature method is presented to examine the bending behavior of the composite structure by considering various boundary conditions. For prediction of the bulk material properties of the multi-scale composite, Halpin–Tsai equations and fiber micromechanics are presented. The carbon nanotubes are supposed to be randomly oriented and uniformly distributed through the matrix of epoxy resin. Afterward, a parametric study is done to present the effects of stacking sequence, various types of sandwich circular/annular plates, linear and torsional gradient elastic foundation, and Biot's coefficient on the bending characteristics of the composite structure. Results reveal that the impact of external pressure on the hoop shear stress, radial stress, and radial shear stress of the laminated circular plate becomes more considerable in the middle layers.

List of symbols

h, R_i, and R_o	Thickness, the inner and outer radius of the disk, respectively
CNTs	Carbon-nanotubes
F and NCM	Fiber and nanocomposite matrix, respectively

[a] e-mail: zhaohu987@163.com
[b] e-mail: wanglinghui0204@163.com (corresponding author)
[c] e-mail: alibek.issakhov@kaznu.kz
[d] e-mail: Hamed_safarpor@yahoo.com

Published online: 09 August 2021

V^{NCM}, V^{F}	Volume fractions of nanocomposite matrix and fiber, respectively
L^{CNT}, T^{CNT}, D^{CNT}, E^{CNT} and V^{CNT}	The length, thickness, diameter, Young's module, and volume fraction of carbon nanotubes, respectively
$V^{*}{}_{\mathrm{CNT}}$, W_{CNT}	Effective volume fraction and weight fraction of the CNTs, respectively
Nt, V_{CNT}	Layer number and volume fraction of CNTs
γ, and P	The Biot's coefficient of effective stress and pore pressure of disk, respectively
ψ, ε, K, K_{u}, k, k_{f}, Φ	The variation of fluid content, volumetric strain, Biots Moduli, undrained bulk modulus, drained bulk modulus, bulk modulus of fluid, and porosity, respectively
$\Im$	Denotes the foundation normal reaction per unit area
$k_w(r,\theta,z)$, $k_p(r,\theta,z)$	The coordinate dependent Winkler–Pasternak coefficients
$k_{\mathrm{wo}}\left(\mathrm{N/m^2\ rad}\right)$, $k_{\mathrm{po}}\left(\mathrm{N/m^2\ rad}\right)$	The elastic coefficients of the Winkler–Pasternak foundation at the center of the bottom surface of the plate
$\Im_r$	Denotes the foundation rotary (shear) reaction per unit area
$k_{r1}(r,\theta)$, $k_{r2}(r,\theta)$	The coordinate dependent torsional stiffness of the foundation
$k_{\mathrm{r10}}\left(\mathrm{Nm/m^2\ rad}\right)$, $k_{\mathrm{r20}}(\mathrm{Nm/m\ rad})$	The torsional coefficients of the foundation at the bottom surface of the plate
f_1, F_2, P_1, and P_2	Parameters describing variations of the normal and shear tractions, respectively
Ξ_{11}, Ξ_{22}, and, Ξ_{33}	Young modulus of CNTs
G^{*}_{12}, G^{*}_{13}, and G^{*}_{23}	Shear modulus of CNTs
υ_{12}, υ_{13}, υ_{23}, υ_{21}, υ_{31}, and υ_{32}	Poison's ratio of CNTs
u_{r}, u_{θ} and u_{z}	The displacements in radial-, circumferential- and axial directions, respectively
$\varepsilon_{\mathrm{ii}}$ and σ_{ii} $(i = r, \theta, Z)$	The components of normal strains and normal stresses
$\gamma_{r\theta}$, γ_{rz}, and $\gamma_{z\theta}$	The components of a shear strains
$\tau_{r\theta}$, τ_{rz}, and $\tau_{z\theta}$	The components of a shear stresses
Q_{ij} and $\bar{Q}_{\mathrm{ij}}$	Stiffness elements, stiffness elements relates to orientation angle and the orientation angle, respectively
θ	The lamination angle with respect to the R axis

1 Introduction

In order to achieve desired thermo-mechanical properties, carbon and its derivatives are accounted as the best choices to reinforce engineering structures [1–3]. Choosing the scale of reinforcement widely depends on the purpose of the engineers [4–11]. Dynamic analysis of composite structures is a key issue in engineering design. Up to now, it is revealed that composites enriched by multi-scales hybrid laminated nanocomposites (MHLNC) are much more beneficial in real engineering applications. So, the dynamic stability of the composites reinforced by MHLNC is a significant area of study. Chakrapani et al. [12] presented a model

of multiple size levels to survey the importance of fiber's, and sequence of laminate's directions on the CF-enriched composite beam's forced oscillation response, which its viscoelasticity was modeled via Kelvin–Voigt equation. Furthermore, they conducted experimental research in order to confirm the accuracy of numerical results. In another study, Ref. [13] presented post-buckling and buckling analysis of the composite beam reinforced by fiber in the hygro-thermal environment with the aid of Reddy's theory. Also, enhancing the mechanical properties of the composite structures using nano-scaled fiber instead of macro-sized ones results in an increase in the mechanics of structures. However, many scientists are focusing on the CNT-reinforced structures. For example, a FE model is applied in order to analyze carbon nanotube reinforced (CNTR) circular and annular plate's buckling relied on higher-order shear deformation theory (HSDT) by Maghamikia et al. [14]. They demonstrated that the critical load determined by their method, when it comes to the buckling investigation, is less than those calculated based on classical methods due to the result of taking into consideration of shear strain terms. Vibration study of continuously graded thick CNTR annular plate lying on an elastic foundation utilizing elasticity model is conducted by Ref. [15], while they used a solution method known as differential quadrature method (DQM) in their research paper. In another study, Tahouneh et al. [16] presented natural frequencies of continuously graded CNTR annular plates lying on an elastic medium in which CNT's weight fraction changes through the plate's thickness, while the elasticity model and DQ method are applied to obtain motion equations and solve those equations, respectively. In both papers reported above, in order to estimate the composite annular plate's elastic properties, Eshelby–Mori–Tanaka micro-scaled mechanics is applied. Ansari et al. [17] presented buckling and frequency analysis of functionally graded CNT-reinforced annular sector plate on the elastic substrate in a thermal environment. This kind of composite structure can be used in many applications [18–21]. In the field of analytical modeling of composite structures, Chen et al. [22] presented buckling and frequency analysis of the FG porous plate via the Chebyshev–Ritz technique. In their research, they showed that FG porosity and boundary conditions have a marvelous effect on the buckling and frequency analysis of the FG porous plate. Frequency information of the annular and circular plates made of 3D graphene foams with the aid of the Chebyshev–Ritz technique was presented by Ref. [23]. Ritz method analysis of rectilinear orthotropic composite circular plates undergoing in-plane bending and torsional moments was studied by Belardi et al. [24]. Reference [25] examined the frequency performance of the conical shell reinforced by CNTs using the kernel particle Ritz element-free method. Frequency information of the membrane assemblies with general classical boundary conditions was presented by Liu et al. [26]. In other work, Belardi et al. [27] studied the radial bending performance of shear-deformable composite circular plates with rectilinear orthotropy. The elastic bending analysis of transversely loaded shear-deformable rectilinear orthotropic composite annular plates via first-order shear deformation (FSDT) was investigated by Ref. [28]. Buckling and free vibration analysis of the highly anisotropic plates via the Ritz method was studied by Vescovini et al. [29]. In their research, they demonstrated that different forms of elastic couplings, boundary conditions, and amount of material anisotropy have important role on the buckling and frequency information of the highly anisotropic plates. The analytical solutions [30–33] and their features presented by Olia et al. [34] provided a fundamental, rational, mechanics-based framework for advancing the understanding of a load transfer mechanism and soil–structure interaction in energy geostructures, thus contributing directly toward better implementing these means of extracting renewable energy sources, which is step forward in reducing the greenhouse gases. In the field of static, bending, and stress–strain responses of the composite structures, Ref. [35] reported a research about the thermostatic information of a simply supported doubly curved shell reinforced by graphene nanoplatelets (GPLs). In

this reference, the state-space governing equations were obtained via 3D elasticity theory. Shaban et al. [36] presented bending responses of an electrically panel that is integrated with a piezoelectric layer. Also, they formulated the problem via elasticity theory and the energy method and solved by using the state-space method. They demonstrated that the geometrical parameters have an important role on the bending responses of an electrically panel. Ref. [37] reported the static and stress–strain responses of an imperfect GPLs reinforced shell via 3D elasticity theory, Halpin–Tsai, and rule of mixture. Their results show that porosity, boundary conditions, and GPLs patterns have important effects on the bending behavior of the inhomogeneous structure. In a comprehensive study, Safarpour et al. [38] had a focus on the static and dynamic behaviors of the GPLs reinforced imperfect circular/annular systems. They derived the formulations of the problem with the aid of the elasticity theory and the Halpin–Tsai model. They employed a semi-numerical method as a solver to draw the results of their paper. Also, Safarpour et al. [39] reported research about the static, bending, and stress–strain responses of the GPLs reinforced cylindrical shell, conical shell, and disk via elasticity theory and generalized differential quadrature (GDQ) method. Alibeigloo et al. [40] presented a paper about the impact of functionally graded (FG) patterns and geometrical parameters of an inhomogeneous shell on the dynamic and static properties via 3D-elasticity theory and Fourier series analytical solution. Ref. [41] had a focus on the static bending performance of the porous size-dependent FG shell via Hamilton's principle and the GDQ method. Their results showed that the length scale factor and imperfection factor have the most remarkable impact on the bending and frequency of the inhomogeneous shell. Parand et al. [42] employed 3D-elasticity theory and the Kelvin–Voigt model to formulate the bending and natural dynamic properties of the viscoelastic FG shell. They used the Fourier series and DQ methods to solve the governing equation of the problem result to show the effect of viscoelastic properties on the static and dynamic behaviors of the inhomogeneous shell. Alibeigloo [43] reported research about the static, bending performance of the time-dependent FG core sandwich simply supported plate under thermal shock. He employed Laplace method to solve the equation of the problem. Do et al. [44] presented the impacts of GPLs patterns on the bending, and dynamic behavior of the cylindrical and spherical panels with the aid of Halpin–Tsai model, higher-order deformation theory, and isogeometric method. Poroelasticity is a continuum theory for the analysis of a porous media consisting of an elastic matrix containing interconnected fluid-saturated pores. In physical terms the theory postulates that when a porous material is subjected to stress, the resulting matrix deformation leads to volumetric changes in the pores. Since the pores are fluid filled, the presence of the fluid not only acts as a stiffener of the material, but also results in the flow of the pore fluid (diffusion) between regions of higher and lower pore pressure. If the fluid is viscous, the behavior of the material system becomes time dependent. The basic phenomenological model for such a material was proposed by Biot [45, 46]. His motivation (and the application of the theory over the years) was concerned with soil consolidation (quasi-static) and wave propagation (dynamic) problems in geomechanics. Rad et al. [47] presented the magneto-elastic analysis of the asymmetric tapered porous FG circular plate on the elastic substrate via 3D elasticity theory. They showed that boundary conditions and elastic foundation have an important role in the stress and displacement fields of the asymmetric tapered porous FG circular plate on the elastic substrate.

According to the best scientific reports, the bending behavior of the MHLNC reinforced axisymmetric circular/annular plates resting on linear and torsional elastic foundation based on three-dimensional poroelasticity theory is not explored yet. In our work, the rule of the mixture and modified Halpin–Tsai model are engaged to provide the effective material constant of the MHLNC reinforced axisymmetric circular/annular plates

(MHLNCRACP/MHLNCRAAP). With the aid of compatibility conditions, the sandwich structure with two, three, five, and seven layers is modeled. The state-space-based differential quadrature method (SS-DQM) is presented to examine the bending behavior of MHLNCRACP/MHLNCRAAP with different boundary conditions. Consequently, a parametric study is done to present the effects of stacking sequence, CNT's distribution pattern, linear and torsional gradient elastic foundation, and Biot's coefficient on the bending characteristics of the sandwich structure.

2 Mathematical modeling

2.1 The homogenization process of MHLNC

For improving the mechanical properties of the structure, we can use of nanoreinforcements [48–52]. The procedure of homogenization is made of two main steps based upon the Halpin–Tsai model [53], together with a micromechanical theory [54], as shown in Fig. 1. The first stage is engaged with computing the effective characteristics of the composite reinforced with CFs as follows [55]

$$\Xi_{11} = V^F \Xi_{11}^F + V^{\mathrm{NCM}} \Xi^{\mathrm{NCM}} \tag{1a}$$

$$\frac{1}{\Xi_{22}} = \frac{V^F}{\Xi_{22}^F} + \frac{V^{\mathrm{NCM}}}{\Xi^{\mathrm{NCM}}} - V^F V^{\mathrm{NCM}} \times \frac{\frac{(v^F)^2 \Xi^{\mathrm{NCM}}}{\Xi_{22}^F} + \frac{(v^{\mathrm{NCM}})^2 \Xi_{22}^F}{\Xi^M} - 2 v^F v^{\mathrm{NCM}}}{V^F \Xi_{22}^F + V^{\mathrm{NCM}} \Xi^{\mathrm{NCM}}} \tag{1b}$$

$$\Xi_{33} = \Xi_{22} \tag{1c}$$

$$\frac{1}{G_{12}^*} = \frac{V^F}{G_{12}^F} + \frac{V^{\mathrm{NCM}}}{G^{\mathrm{NCM}}}, \quad G_{23}^* = G_{12}^*, \quad G_{13}^* = G_{12}^* \tag{1d}$$

$$\upsilon_{12} = V^{\mathrm{F}} v^{\mathrm{F}} + V^{\mathrm{NCM}} v^{\mathrm{NCM}} \tag{1e}$$

$$\upsilon_{21} = \frac{\Xi_{22}}{\Xi_{11}} \upsilon_{12}, \quad \upsilon_{13} = \upsilon_{12}, \quad \upsilon_{31} = \upsilon_{21}, \quad \upsilon_{32} = \upsilon_{21}, \quad \upsilon_{23} = \upsilon_{32} \tag{1f}$$

The relation between V^{F} and V^{NCM} is as follows [55]:

$$V^F + V^{\mathrm{NCM}} = 1 \tag{2}$$

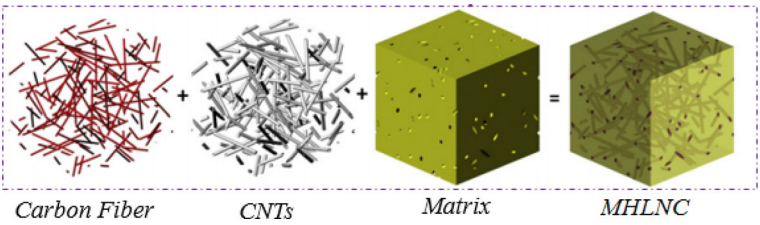

Fig. 1 Distribution patterns of CNT through the thickness of the MHLNC

The second step is organized to obtain the effective characteristics of the nanocomposite matrix reinforced with CNTs with the aid of the extended Halpin–Tsai micromechanics as follows [56]:

$$\Xi^{\mathrm{NCM}} = \Xi^{\mathrm{M}}\left(\frac{5}{8}\left(\frac{1+2\xi_{\mathrm{dd}}V^{\mathrm{CNT}}}{1-\xi_{\mathrm{dd}}V^{\mathrm{CNT}}}\right) + \frac{3}{8}\left(\frac{1+2(l^{\mathrm{CNT}}/d^{\mathrm{CNT}})\xi_{\mathrm{dl}}V^{\mathrm{CNT}}}{1-\xi_{\mathrm{dl}}V^{\mathrm{CNT}}}\right)\right) \tag{3}$$

Here ξ_{dd} and ξ_{dl} are computed as the following expressions:

$$\begin{aligned}\xi_{\mathrm{dl}} &= \frac{(\Xi_{11}^{\mathrm{CNT}}/\Xi^{\mathrm{M}}) - (D^{\mathrm{CNT}}/4T^{\mathrm{CNT}})}{(\Xi_{11}^{\mathrm{CNT}}/\Xi^{\mathrm{M}}) + (L^{\mathrm{CNT}}/2T^{\mathrm{CNT}})},\\ \xi_{\mathrm{dd}} &= \frac{(\Xi_{11}^{\mathrm{CNT}}/\Xi^{\mathrm{M}}) - (D^{\mathrm{CNT}}/4T^{\mathrm{CNT}})}{(\Xi_{11}^{\mathrm{CNT}}/\Xi^{\mathrm{M}}) + (D^{E}/2T^{\mathrm{CNT}})}\end{aligned} \tag{4}$$

the volume fraction of CNTs can be formulated as follows [57]:

$$V_{*}^{\mathrm{CNT}} = \frac{W^{\mathrm{CNT}}}{W^{\mathrm{CNT}} + (\frac{\rho^{\mathrm{CNT}}}{\rho^{\mathrm{M}}})(1-W^{\mathrm{CNT}})} \tag{5}$$

Also, MHLNC distribution, along with thickness direction, can be given by [58]:

$$V^{\mathrm{CNT}} = V_{*}^{\mathrm{CNT}} \tag{6}$$

In addition, the relation between V^{M} and V^{CNT} is as follows [59]:

$$V^{\mathrm{CNT}} + V^{\mathrm{M}} = 1 \tag{7}$$

Finally, the mechanical properties of the nanocomposite structure can be given by [59]:

$$\nu^{\mathrm{NCM}} = \nu^{\mathrm{M}} \tag{8a}$$

$$G^{NCM} = \frac{\Xi^{\mathrm{NCM}}}{2\left(1+\nu^{\mathrm{NCM}}\right)} \tag{8b}$$

3 Formulation of basic equations

Consider an MHLNCRACP/MHLNCRAAP as shown in Fig. 2. Three-dimensional governing differential equation of motion in the absence of body forces is [60]

$$\sigma_{r,r} + \tau_{rz,z} + r^{-1}\tau_{r\theta,\theta} + (\sigma_r - \sigma_\theta)r^{-1} = 0 \tag{9a}$$

$$\tau_{r\theta,r} + \tau_{\theta z,z} + r^{-1}\sigma_{\theta,\theta} + 2r^{-1}\tau_{r\theta} = 0 \tag{9b}$$

$$\tau_{rz,r} + \sigma_{z,z} + r^{-1}\tau_{\theta z,\theta} + r^{-1}\tau_{rz} = 0 \tag{9c}$$

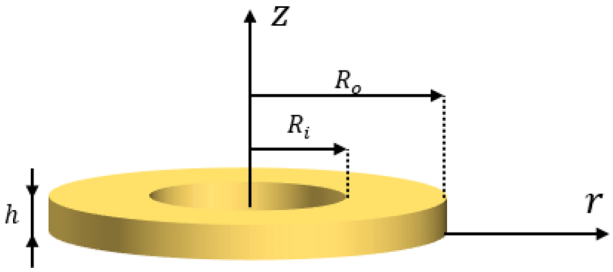

Fig. 2 Schematic view of the MHLNC

Poroelasticity is a continuum theory for the analysis of porous media consisting of an elastic matrix containing interconnected fluid-saturated pores. Stress–strain relations of MHC cross-ply laminated circular/annular plates of poroelasticity can be written as follows [61]:

$$\begin{Bmatrix} \sigma_{rr} \\ \sigma_{\theta\theta} \\ \sigma_{zz} \\ \tau_{z\theta} \\ \tau_{rz} \\ \tau_{r\theta} \end{Bmatrix} = \begin{bmatrix} \overline{Q}_{11} & \overline{Q}_{12} & \overline{Q}_{13} & 0 & 0 & 0 \\ \overline{Q}_{12} & \overline{Q}_{22} & \overline{Q}_{23} & 0 & 0 & 0 \\ \overline{Q}_{13} & \overline{Q}_{23} & \overline{Q}_{33} & 0 & 0 & 0 \\ & & & \overline{Q}_{44} & 0 & 0 \\ & \text{sym.} & & 0 & \overline{Q}_{55} & 0 \\ & & & 0 & 0 & \overline{Q}_{66} \end{bmatrix} \begin{Bmatrix} \varepsilon_{rr} \\ \varepsilon_{\theta\theta} \\ \varepsilon_{zz} \\ \gamma_{z\theta} \\ \gamma_{rz} \\ \gamma_{r\theta} \end{Bmatrix} - \begin{Bmatrix} \gamma P \\ \gamma P \\ \gamma P \\ 0 \\ 0 \\ 0 \end{Bmatrix} \tag{10}$$

where [61]

$$\overline{Q}_{11} = \alpha^4 Q_{22} + 2\alpha^2\beta^2(Q_{12} + 2Q_{66}) + \beta^4 Q_{11} \tag{11a}$$

$$\overline{Q}_{12} = \left(\alpha^4 + \beta^4\right)Q_{12} + \alpha^2\beta^2(Q_{22} + Q_{11} - 4Q_{66}) \tag{11b}$$

$$\overline{Q}_{13} = \alpha^2 Q_{23} + \beta^2 Q_{13},\ \overline{Q}_{22} = \alpha^4 Q_{11} + \beta^4 Q_{22} + 2\alpha^2\beta^2(Q_{12} + 2Q_{66}) \tag{11c}$$

$$\overline{Q}_{23} = \beta^2 Q_{23} + \alpha^2 Q_{13},\ \overline{Q}_{33} = Q_{33},\ \overline{Q}_{44} = \alpha^2 Q_{55} + \beta^2 Q_{44} \tag{11d}$$

$$\begin{aligned} \overline{Q}_{55} &= \alpha^2 Q_{44} - 2\alpha\beta Q_{45} + \beta^2 Q_{55}, \\ \overline{Q}_{66} &= Q_{66}\left(\beta^2 - \alpha^2\right)^2 - 4\alpha^2\beta^2(2Q_{12} - Q_{11} - Q_{22}) \end{aligned} \tag{11e}$$

where $\alpha = \sin(\theta)$, and $\beta = \cos(\theta)$. Also [62–67]

$$\begin{aligned} Q_{11} &= \frac{(1 - v_{32}v_{23})}{\Upsilon}\Xi_{11}\,, \quad Q_{12} = \frac{(v_{21} + v_{23}v_{31})}{\Upsilon}\Xi_{11}\,, \\ Q_{13} &= \frac{(v_{31} + v_{32}v_{21})}{\Upsilon}\Xi_{11}, \end{aligned} \tag{12a}$$

$$\begin{aligned} Q_{22} &= \frac{(1 - v_{31}v_{13})}{\Upsilon}\Xi_{22}\,, \quad Q_{23} = \frac{(v_{32} + v_{31}v_{12})}{\Upsilon}\Xi_{22}\,, \\ Q_{33} &= \frac{(1 - v_{21}v_{12})}{\Upsilon}\Xi_{33} \end{aligned} \tag{12b}$$

$$Q_{66} = G^*_{13}\,, \quad Q_{55} = G^*_{23}, \quad Q_{44} = G^*_{12} \tag{12c}$$

$$\Upsilon = (1 - v_{32}v_{23} - v_{21}v_{12} - v_{31}v_{13} - 2v_{23}v_{31}v_{12}) \tag{12d}$$

The strains of the MHLNCRCP/MHLNCRAP can be written as follows [38]:

$$\varepsilon_{\mathrm{r}} = \frac{\partial u_{\mathrm{r}}}{\partial r},\ \varepsilon_{\theta} = \frac{1}{r}\left(\frac{\partial u_{\theta}}{\partial \theta} + u_{\mathrm{r}}\right),\ \varepsilon_{\mathrm{z}} = \frac{\partial u_{\mathrm{z}}}{\partial z}, \tag{13a}$$

$$\gamma_{r\theta} = \frac{1}{r}\frac{\partial u_r}{\partial \theta} + \frac{\partial u_\theta}{\partial r} - \frac{u_\theta}{r}, \quad \gamma_{rz} = \frac{\partial u_r}{\partial z} + \frac{\partial u_z}{\partial r}, \quad \gamma_{\theta z} = \frac{\partial u_\theta}{\partial z} + \frac{1}{r}\frac{\partial u_z}{\partial \theta} \tag{13b}$$

The other parameter in Eq. (10) is written as follows:

$$P = K^P(\psi - (\varepsilon_{\mathrm{rr}} + \varepsilon_{\theta\theta} + \varepsilon_{\mathrm{zz}})\gamma) \tag{14a}$$

$$K^P = -\frac{(k - k_u)}{\gamma^2} \tag{14b}$$

$$k_{\mathrm{u}} = \left[1 - \frac{k_{\mathrm{f}}\gamma^2}{(\phi - \gamma)(1 - \gamma)k_{\mathrm{f}} + k_{\mathrm{f}}\phi}\right]k \tag{14c}$$

In Eq. (14a), parameter $\psi = 0$ for undrained conditions; the constants become [68]:

$$P = -K^P\varepsilon\gamma = -K^P(\varepsilon_{\mathrm{rr}} + \varepsilon_{\theta\theta} + \varepsilon_{\mathrm{zz}})\gamma \tag{15}$$

The substitution of Eqs. (15) into (10) gives

$$\begin{bmatrix} \sigma_{rr} \\ \sigma_{\theta\theta} \\ \sigma_{zz} \\ \tau_{\theta z} \\ \tau_{rz} \\ \tau_{r\theta} \end{bmatrix} = \begin{bmatrix} \overline{Q}^*_{11} & \overline{Q}^*_{12} & \overline{Q}^*_{13} & 0 & 0 & 0 \\ \overline{Q}^*_{12} & \overline{Q}^*_{22} & \overline{Q}^*_{23} & 0 & 0 & 0 \\ \overline{Q}^*_{13} & \overline{Q}^*_{23} & \overline{Q}^*_{33} & 0 & 0 & 0 \\ & & & \overline{Q}_{44} & 0 & 0 \\ & \text{sym.} & & 0 & \overline{Q}_{55} & 0 \\ & & & 0 & 0 & \overline{Q}_{66} \end{bmatrix} \begin{bmatrix} \frac{\partial u_r}{\partial r} \\ \frac{1}{r}\left(\frac{\partial u_\theta}{\partial \theta} + u_r\right) \\ \frac{\partial u_z}{\partial z} \\ \frac{\partial u_\theta}{\partial z} + \frac{1}{r}\frac{\partial u_z}{\partial \theta} \\ \frac{\partial u_r}{\partial z} + \frac{\partial u_z}{\partial r} \\ \frac{1}{r}\frac{\partial u_r}{\partial \theta} + \frac{\partial u_\theta}{\partial r} - \frac{u_\theta}{r} \end{bmatrix} \tag{16}$$

where

$$\overline{Q}^*_{ij} = \overline{Q}_{ij} + K^P\gamma^2; \quad i = j = 1, 2, 3 \tag{17}$$

By using Eqs. (9a–c) and (16) as below:

$$\sigma_{z,z} = -\tau_{rz,r} - r^{-1}\tau_{rz} + r^{-1}\tau_{z\theta,\theta}, \tag{18a}$$

$$u_{\mathrm{r,z}} = -u_{\mathrm{z,r}} + \frac{\tau_{\mathrm{rz}}}{\overline{Q}_{55}} \tag{18b}$$

$$u_{\theta,z} = -r^{-1}u_{z,\theta} + \frac{\tau_{z\theta}}{\overline{Q}_{44}}, \tag{18c}$$

$$u_{z,z} = \frac{\sigma_z}{\overline{Q}^*_{33}} - \frac{\overline{Q}^*_{13}}{\overline{Q}^*_{33}}u_{r,r} - r^{-1}\frac{\overline{Q}^*_{23}}{\overline{Q}^*_{33}}u_r - r^{-1}\frac{\overline{Q}^*_{23}}{\overline{Q}^*_{33}}u_{\theta,\theta} \tag{18d}$$

$$\begin{aligned} \tau_{rz,z} = &-\frac{\bar{Q}^*_{13}}{\bar{Q}^*_{33}}\sigma_{z,r} - \left(\frac{\bar{Q}^*_{13} - \bar{Q}^*_{23}}{\bar{Q}^*_{33}}\right)\sigma_z - \left(\bar{Q}^*_{11} - \frac{\bar{Q}^{*2}_{13}}{\bar{Q}^*_{33}}\right)u_{r,rr} \\ &- r^{-1}\left(\bar{Q}^*_{11} - \frac{\bar{Q}^{*2}_{13}}{\bar{Q}^*_{33}}\right)u_{r,r} - r^{-2}\bar{Q}_{66}u_{r,\theta\theta} \\ &- r^{-2}\left(\frac{\bar{Q}^*_{12}\bar{Q}^*_{33} + \bar{Q}^{*2}_{23} - \bar{Q}^*_{13}\bar{Q}^*_{23} - \bar{Q}^*_{22}\bar{Q}^*_{33}}{\bar{Q}^*_{33}}\right)u_r \end{aligned}$$

$$- r^{-1}\left(\bar{Q}^*_{12} + \bar{Q}_{66} - \frac{\bar{Q}^*_{13}\bar{Q}^*_{23}}{\bar{Q}^*_{33}}\right)u_{\theta,r\theta}$$
$$- r^{-2}\left(\frac{\bar{Q}^*_{12}\bar{Q}^*_{33} + \bar{Q}^{*2}_{23} - \bar{Q}^*_{13}\bar{Q}^*_{23} - \bar{Q}^*_{22}\bar{Q}^*_{33}}{\bar{Q}^*_{33}}\right)u_{\theta,\theta} \tag{18e}$$

$$\tau_{\theta z,z} = - r^{-1}\frac{\bar{Q}^*_{23}}{\bar{Q}^*_{33}}\sigma_{z,\theta} - r^{-1}\left(\bar{Q}^*_{12} + \bar{Q}_{66} - \frac{\bar{Q}^*_{13}\bar{Q}^*_{23}}{\bar{Q}^*_{33}}\right)u_{r,r\theta}$$
$$- r^{-2}\left(\bar{Q}^*_{22} + 2\bar{Q}_{66} - \frac{\bar{Q}^{*2}_{23}}{\bar{Q}^*_{33}}\right)u_{r,\theta}$$
$$- \bar{Q}_{66}u_{\theta,rr} - \frac{\bar{Q}_{66}}{r}u_{\theta,r}$$
$$- r^{-2}\left(\bar{Q}^*_{22} - \frac{\bar{Q}^{*2}_{23}}{\bar{Q}^*_{33}}\right)u_{\theta,\theta\theta} + 2r^{-2}\bar{Q}_{66}u_\theta \tag{18f}$$

The matrix form Eqs. (18a–f) can be written as follows:

$$\frac{\mathrm{d}\boldsymbol{\delta}}{\mathrm{d}z} = \mathbf{G}\delta \tag{19}$$

where $\delta = \{\sigma_z\ u_r\ u_\theta\ u_z\ \tau_{rz}\ \tau_{\theta z}\}^T$ is the state variable vector and G is the coefficients matrix which is given as

$$G = \begin{bmatrix} 0 & 0 & 0 & 0 & -\frac{\partial}{\partial r} - \frac{1}{r} & \frac{1}{r}\frac{\partial}{\partial\theta} \\ 0 & 0 & 0 & -\frac{\partial}{\partial r} & \frac{1}{\overline{Q}_{55}} & 0 \\ 0 & 0 & 0 & -\frac{1}{r}\frac{\partial}{\partial\theta} & 0 & \frac{1}{\overline{Q}_{44}} \\ \frac{\sigma_z}{\overline{Q}^*_{33}} & -\frac{\overline{Q}^*_{13}}{\overline{Q}^*_{33}}\frac{\partial}{\partial r} - r^{-1}\frac{\overline{Q}^*_{23}}{\overline{Q}^*_{33}} & -r^{-1}\frac{\overline{Q}^*_{23}}{\overline{Q}^*_{33}}\frac{\partial}{\partial\theta} & 0 & 0 & 0 \\ G_{51} & G_{52} & G_{53} & 0 & 0 & 0 \\ -r^{-1}\frac{\overline{Q}^*_{23}}{\overline{Q}^*_{33}}\frac{\partial}{\partial\theta} & G_{62} & G_{63} & 0 & 0 & 0 \end{bmatrix} \tag{20}$$

where

$$G_{51} = -\frac{\overline{Q}^*_{13}}{\overline{Q}^*_{33}}\frac{\partial}{\partial r} - \left(\frac{\overline{Q}^*_{13} - \overline{Q}^*_{23}}{\overline{Q}^*_{33}}\right) \tag{21a}$$

$$G_{52} = -\left(\overline{Q}^*_{11} - \frac{\overline{Q}^{*2}_{13}}{\overline{Q}^*_{33}}\right)\frac{\partial^2}{\partial r^2} - r^{-1}\left(\overline{Q}^*_{11} - \frac{\overline{Q}^{*2}_{13}}{\overline{Q}^*_{33}}\right)\frac{\partial}{\partial r} - r^{-2}\overline{Q}_{66}\frac{\partial^2}{\partial\theta^2}$$
$$- r^{-2}\left(\frac{\overline{Q}^*_{12}\overline{Q}^*_{33} + \overline{Q}^{*2}_{23} - \overline{Q}^*_{13}\overline{Q}^*_{23} - \overline{Q}^*_{22}\overline{Q}^*_{33}}{\overline{Q}^*_{33}}\right) \tag{21b}$$

$$G_{53} = - r^{-1}\left(\bar{Q}^*_{12} + \bar{Q}_{66} - \frac{\bar{Q}^*_{13}\bar{Q}^*_{23}}{\bar{Q}^*_{33}}\right)\frac{\partial^2}{\partial r\partial\theta}$$
$$- r^{-2}\left(\frac{\bar{Q}^*_{12}\bar{Q}^*_{33} + \bar{Q}^{*2}_{23} - \bar{Q}^*_{13}\bar{Q}^*_{23} - \bar{Q}^*_{22}\bar{Q}^*_{33}}{\bar{Q}^*_{33}}\right)\frac{\partial}{\partial\theta} \tag{21c}$$

$$G_{62} = -r^{-1}\left(\overline{Q}^*_{12} + \overline{Q}_{66} - \frac{\overline{Q}^*_{13}\overline{Q}^*_{23}}{\overline{Q}^*_{33}}\right)\frac{\partial^2}{\partial r\partial\theta} - r^{-2}\left(\overline{Q}^*_{22} + 2\overline{Q}_{66} - \frac{\overline{Q}^{*2}_{23}}{\overline{Q}^*_{33}}\right)\frac{\partial}{\partial\theta} \tag{21d}$$

$$G_{63} = -\overline{Q}_{66}\frac{\partial^2}{\partial r^2} - \frac{\overline{Q}_{66}}{r}\frac{\partial}{\partial r} - r^{-2}\left(\overline{Q}^*_{22} - \frac{\overline{Q}^{*2}_{23}}{\overline{Q}^*_{33}}\right)\frac{\partial^2}{\partial\theta^2} + 2r^{-2}\overline{Q}_{66} \tag{21e}$$

And the relations for different boundary conditions can be formulated as follows:

$$\text{Simply} : \sigma_r = u_z = u_\theta = 0, \quad \text{Clamped} : u_r = u_z = u_\theta = 0 \tag{22}$$

Also, for circular plate at $r = 0$:

$$u_r = u_{z,r} = u_{\theta,r} = 0 \quad r = 0 \tag{23}$$

4 The linear and torsional elastic foundation

The Winkler–Pasternak foundations for MHLNCRACP/MHLNCRAAP can be written as follows:

$$\Im = k_w(r,\theta,z)u_z - r^{-1}\left(rk_p(r,\theta,z)u_{z,r}\right)_{,r} - r^{-2}\left(k_p(r,\theta,z)u_{z,\theta}\right)_{,r} \tag{24}$$

These parameters of Eq. (24) can be written as follows:

$$k_{\mathrm{w}}(r,\theta,z) = k_{\mathrm{wo}}\left(1 + f_1\left(\frac{r}{R_o}\right) + f_2\left(\frac{r}{R_o}\right)^2\right)\cos(\theta_0) \tag{25a}$$

$$k_{\mathrm{p}}(r,\theta,z) = k_{\mathrm{po}}\left(1 + f_1\left(\frac{r}{R_o}\right) + f_2\left(\frac{r}{R_o}\right)^2\right)\cos(\theta_0) \tag{25b}$$

The torsional elastic foundation can be written as follows:

$$\Im_r = k_{r1}(r,\theta)\phi - r^{-1}\left(rk_{r2}(r,\theta)\phi_{,r}\frac{\partial}{\partial r}\right)_{,r} \tag{26}$$

Substituting $\phi = u_{\theta,r}$ into Eq. (26) leads to:

$$\Im_r = k_{r1}(r,\theta)u_{\theta,r} - r^{-1}\left(rk_{r2}(r,\theta)u_{\theta,rr}\frac{\partial^2}{\partial r^2}\right)_{,r} \tag{27}$$

These coefficients are considered as

$$k_{r1}(r,\theta) = k_{r10}\left(1 + P_1\left(\frac{r}{R_o}\right) + P_2\left(\frac{r}{R_o}\right)^2\right)\sin(\theta_0) \tag{28a}$$

$$k_{r2}(r,\theta,z) = k_{r20}\left(1 + P_1\left(\frac{r}{R_o}\right) + P_2\left(\frac{r}{R_o}\right)^2\right)\sin(\theta_0) \tag{28b}$$

5 Solution procedure

To solve the state-space Eq. (18a–f), the differential quadrature method (DQM) is employed [69]. The basic idea of DQM is to approximate an unknown function and its partial derivatives with respect to a spatial variable at any discrete point as the linear weighted sums of their

values at all the discrete points chosen in the solution domain. In this method, the rth-order derivative of an unknown function $f(r)$ at point i can be expressed as [70–74]:

$$\frac{\partial^n f(r)}{\partial r^n} = \sum_{j=1}^{M} g_{ij}^{(n)} f\left(r_j\right); \quad n = 1, ..., N \tag{29}$$

where N is the total number of discrete points, r_j is the coordinate of discrete point j, $f\left(r_j\right)$ is the function value at the discrete point j, and $g_{ij}^{(n)}$ is a weighting coefficient matrix of nth-order derivative.

Also, displacement and stress fields of an MHLNCRACP/MHLNCRAAP can be given by:

$$u_r = \sum_{m=1}^{\infty} \hat{u}_r \sin(\theta m), \ u_\theta = \sum_{m=1}^{\infty} \hat{u}_\theta \cos(\theta m), \ u_z = \sum_{m=1}^{\infty} \hat{u}_z \sin(\theta m), \tag{30a}$$

$$\sigma_r = \sum_{m=1}^{\infty} \hat{\sigma}_r \sin(\theta m), \ \sigma_\theta = \sum_{m=1}^{\infty} \hat{\sigma}_\theta \sin(\theta m), \ \sigma_z = \sum_{m=1}^{\infty} \hat{\sigma}_z \sin(\theta m), \tag{30b}$$

$$\tau_{rz} = \sum_{m=1}^{\infty} \hat{\tau}_{rz} \sin(\theta m), \ \tau_{r\theta} = \sum_{m=1}^{\infty} \hat{\tau}_{r\theta} \cos(\theta m), \ \tau_{\theta z} = \sum_{m=1}^{\infty} \hat{\tau}_{\theta z} \cos(\theta m) \tag{30c}$$

By applying Eqs. (30a–c), and (29) to Eq. (18a–f), the derivatives along the radial direction are removed from the final equation, and only the first-order derivatives with respect to thickness remain. Thus, the discretized state-space equations at an arbitrary discrete point r_j are derived as

$$\frac{\partial \hat{\sigma}_{zi}}{\partial \bar{z}} = -\sum_{j=1}^{N} g_{ij} \hat{\tau}_{rzj} - \frac{\hat{\tau}_{rzi}}{r_i} - \frac{m}{r_i} \hat{\tau}_{z\theta i}, \tag{31a}$$

$$\frac{\partial \hat{u}_{ri}}{\partial \bar{z}} = -\sum_{j=1}^{N} g_{ij} \hat{u}_{zj} + \frac{\hat{\tau}_{rzi}}{\overline{Q}_{55}} \tag{31b}$$

$$\frac{\partial \hat{u}_{\theta i}}{\partial \bar{z}} = -\frac{1}{r_i} m \hat{u}_{zi} + \frac{\hat{\tau}_{z\theta i}}{\overline{Q}_{44}}, \tag{31c}$$

$$\frac{\partial \hat{u}_{zi}}{\partial z} = \frac{\hat{\sigma}_{zi}}{\overline{Q}_{33}^*} - \frac{\overline{Q}_{13}^*}{\overline{Q}_{33}^*} \sum_{j=1}^{N} g_{ij} \hat{u}_{rj} - \frac{\overline{Q}_{23}^*}{r_i \overline{Q}_{33}^*} \hat{u}_{ri} + \frac{m \overline{Q}_{23}^*}{r_i \overline{Q}_{33}^*} \hat{u}_{\theta i} \tag{31d}$$

$$\begin{aligned}
\frac{\partial \hat{\tau}_{rzi}}{\partial \bar{z}} = & -\frac{\bar{Q}_{13}^*}{\bar{Q}_{33}^*} \sum_{j=1}^{N} g_{ij} \hat{\sigma}_{zj} - \frac{1}{r_i} \left(\frac{\bar{Q}_{13}^* - \bar{Q}_{23}^*}{\bar{Q}_{33}^*} \right) \hat{\sigma}_{zi} \\
& - \left(\bar{Q}_{11}^* - \frac{\bar{Q}_{13}^{*2}}{\bar{Q}_{33}^*} \right) \sum_{j=1}^{N} g_{ij}^2 \hat{u}_{rj} \\
& - \frac{1}{r_i} \left(\bar{Q}_{11}^* - \frac{\bar{Q}_{13}^{*2}}{\bar{Q}_{33}^*} \right) \sum_{j=1}^{N} g_{ij} \hat{u}_{rj} + m^2 \frac{\bar{Q}_{66}}{r_i^2} \hat{u}_{ri} \\
& - \frac{1}{r_i^2} \left(\frac{\bar{Q}_{12}^* \bar{Q}_{33}^* + \bar{Q}_{23}^{*2} - \bar{Q}_{13}^* \bar{Q}_{23}^* - \bar{Q}_{22}^* \bar{Q}_{33}^*}{\bar{Q}_{33}^*} \right) \hat{u}_{ri} \\
& + \frac{m}{r_i} \left(\bar{Q}_{12}^* + \bar{Q}_{66} - \frac{\bar{Q}_{13}^* \bar{Q}_{23}^*}{\bar{Q}_{33}^*} \right) \sum_{j=1}^{N} g_{ij} \hat{u}_{\theta j}
\end{aligned}$$

$$+\frac{m^2}{r_i^2}\left(\frac{\bar{Q}_{12}^*\bar{Q}_{33}^*+\bar{Q}_{23}^{*2}-\bar{Q}_{13}^*\bar{Q}_{23}^*-\bar{Q}_{22}^*\bar{Q}_{33}^*}{\bar{Q}_{33}^*}\right)\hat{u}_{\theta i} \tag{31e}$$

$$\frac{\partial\tau_{\theta zi}}{\partial z}=-\frac{m}{r_i}\frac{\bar{Q}_{23}^*}{\bar{Q}_{33}^*}\hat{\sigma}_{zi}-\frac{m}{r_i}\left(\bar{Q}_{12}^*+\bar{Q}_{66}-\frac{\bar{Q}_{13}^*\bar{Q}_{23}^*}{\bar{Q}_{33}^*}\right)\sum_{j=1}^{N}g_{ij}\hat{u}_{rj}$$
$$-\frac{m}{r_i^2}\left(\bar{Q}_{22}^*+2\bar{Q}_{66}-\frac{\bar{Q}_{23}^{*2}}{\bar{Q}_{33}^*}\right)\hat{u}_{ri}-\bar{Q}_{66}\sum_{j=1}^{N}g_{ij}^2\hat{u}_{\theta j}-\frac{\bar{Q}_{66}}{r_i}\sum_{j=1}^{N}g_{ij}\hat{u}_{\theta j}$$
$$+\frac{m^2}{r_i^2}\left(\bar{Q}_{22}^*-\frac{\bar{Q}_{23}^{*2}}{\bar{Q}_{33}^*}\right)\hat{u}_{\theta i}+\frac{2\bar{Q}_{66}}{r_i^2}\hat{u}_{\theta i} \tag{31f}$$

where $i, j = 1, 2, \ldots, N$, $A_{ij} = g_{ij}^{(1)}$, and $B_{ij} = g_{ij}^{(2)}$ are the weighting coefficients of the first- and second-order derivatives with respect to and can be obtained as [75–79]:

$$A_{ij}=\begin{cases}\frac{\prod_{k=1,k\neq i,j}^{N}(r_i-r_k)}{\prod_{k=1,k\neq i,j}^{N}(r_j-r_k)} & i\neq j\\ \frac{1}{\sum_{k=1,k\neq i,j}^{N}(r_j-r_k)} & i=j\end{cases} \tag{32}$$
$$B_{ij}=\sum_{k=1}^{N}A_{ik}A_{kj}\quad i,j=1,...,N$$

Also, using Chebyshev polynomials grid points, the seed along with r-axes can be distributed as [80]:

$$r_i=\frac{R_0-R_i}{2}\left(1-\cos\left(\frac{(i-1)}{(N_i-1)}\pi\right)\right)+R_i\quad i=1,2,3,\ \ldots,N \tag{33}$$

For convenience, the following dimensionless physical quantities are introduced

$$\left(\overline{\sigma}_z\ \overline{\sigma}_r\ \overline{\sigma}_\theta\ \overline{\tau}_{rz}\ \overline{\tau}_{r\theta}\ \overline{\tau}_{\theta z}\right)=\frac{1}{E_m}\left(\hat{\sigma}_z\ \hat{\sigma}_r\ \hat{\sigma}_\theta\ \hat{\tau}_{rz}\ \hat{\tau}_{r\theta}\ \hat{\tau}_{\theta z}\right),\ \overline{E}=\frac{E}{P_0} \tag{34a}$$

$$\left(\overline{U}_r\ \overline{U}_\theta\ \overline{U}_z\right)=\frac{1}{h}\left(u_r\ u_\theta\ u_z\right),\ \overline{r}=\frac{r}{R_m},\ \overline{Z}=\frac{Z}{h} \tag{34b}$$

$$\hat{\overline{Q}}_{\mathrm{ij}}=\frac{\overline{Q}_{\mathrm{ij}}}{P_0},\ \overline{g}_{\mathrm{ij}}=g_{\mathrm{ij}}R_{\mathrm{m}},\ \overline{p}=\frac{q}{P_0},\ P_0=1\ [\mathrm{Mpa}] \tag{34c}$$

Substitution of Eqs. (34a–c) into Eq. (31a–f):

$$\frac{\partial\overline{\sigma}_{zi}}{\partial\overline{z}}=-\frac{h}{R_m}\sum_{j=1}^{N}\overline{g}_{ij}\overline{\tau}_{rzj}-\frac{h}{R_m}\frac{\overline{\tau}_{rzi}}{\overline{r}_i}-\frac{h}{R_m}\frac{m}{\overline{r}_i}\overline{\tau}_{z\theta i}, \tag{35a}$$

$$\frac{\partial\overline{u}_{ri}}{\partial\overline{z}}=-\frac{h}{R_m}\sum_{j=1}^{N}\overline{g}_{ij}\overline{u}_{zj}+\frac{\overline{\tau}_{rzi}}{\hat{\overline{Q}}_{55}} \tag{35b}$$

$$\frac{\partial\overline{u}_{\theta i}}{\partial\overline{z}}=-\frac{h}{R_m}\frac{1}{\overline{r}_i}m\overline{u}_{zi}+\frac{\overline{\tau}_{z\theta i}}{\hat{\overline{Q}}_{44}}, \tag{35c}$$

$$\frac{\partial\overline{u}_{zi}}{\partial\overline{z}}=\frac{\overline{\sigma}_{zi}}{\hat{\overline{Q}}_{33}}-\frac{h}{R_m}\frac{\hat{\overline{Q}}_{13}}{\hat{\overline{Q}}_{33}}\sum_{j=1}^{N}\overline{g}_{ij}\overline{u}_{rj}-\frac{h}{R_m}\frac{\hat{\overline{Q}}_{23}}{\overline{r}_i\hat{\overline{Q}}_{33}}\overline{u}_{ri}+\frac{h}{R_m}\frac{m\hat{\overline{Q}}_{23}}{\overline{r}_i\hat{\overline{Q}}_{33}}\overline{u}_{\theta i} \tag{35d}$$

$$\frac{\partial \overline{\tau}_{rzi}}{\partial \overline{z}} = -\frac{h}{R_m}\frac{\hat{\overline{Q}}_{13}}{\hat{\overline{Q}}_{33}}\sum_{j=1}^{N} g_{ij}\sigma_{zj} - \frac{h}{R_m}\frac{1}{\overline{r}_i}\left(\frac{\hat{\overline{Q}}_{13}-\hat{\overline{Q}}_{23}}{\hat{\overline{Q}}_{33}}\right)\sigma_{zi} - \left(\frac{h}{R_m}\right)^2\left(\hat{\overline{Q}}_{11}-\frac{\hat{\overline{Q}}_{13}^2}{\hat{\overline{Q}}_{33}}\right)\sum_{j=1}^{N}\overline{g}_{ij}^2\overline{u}_{rj} - \left(\frac{h}{R_m}\right)^2\frac{1}{\overline{r}_i}\left(\hat{\overline{Q}}_{11}-\frac{\hat{\overline{Q}}_{13}^2}{\hat{\overline{Q}}_{33}}\right)\sum_{j=1}^{N}\overline{g}_{ij}\overline{u}_{rj} + m^2\frac{\hat{\overline{Q}}_{66}}{\overline{r}_i^2}\overline{u}_{ri} - \left(\frac{h}{R_m}\right)^2\frac{1}{\overline{r}_i^2}\left(\frac{\hat{\overline{Q}}_{12}\hat{\overline{Q}}_{33}+\hat{\overline{Q}}_{23}^2-\hat{\overline{Q}}_{13}\hat{\overline{Q}}_{23}-\hat{\overline{Q}}_{22}\hat{\overline{Q}}_{33}}{\hat{\overline{Q}}_{33}}\right)\overline{u}_{ri} + \left(\frac{h}{R_m}\right)^2\frac{m}{\overline{r}_i}\left(\hat{\overline{Q}}_{12}+\hat{\overline{Q}}_{66}-\frac{\hat{\overline{Q}}_{13}\hat{\overline{Q}}_{23}}{\hat{\overline{Q}}_{33}}\right)\sum_{j=1}^{N}\overline{g}_{ij}\overline{u}_{\theta j} + \left(\frac{h}{R_m}\right)^2\frac{m^2}{\overline{r}_i^2}\left(\frac{\hat{\overline{Q}}_{12}\hat{\overline{Q}}_{33}+\hat{\overline{Q}}_{23}^2-\hat{\overline{Q}}_{13}\hat{\overline{Q}}_{23}-\hat{\overline{Q}}_{22}\hat{\overline{Q}}_{33}}{\hat{\overline{Q}}_{33}}\right)\overline{u}_{\theta i} \tag{35e}$$

$$\frac{\partial \overline{\tau}_{\theta zi}}{\partial \overline{z}} = -\frac{h}{R_m}\frac{m}{\overline{r}_i}\frac{\hat{\overline{Q}}_{23}}{\hat{\overline{Q}}_{33}}\overline{\sigma}_{zi} - \left(\frac{h}{R_m}\right)^2\frac{m}{\overline{r}_i}\left(\hat{\overline{Q}}_{12}+\hat{\overline{Q}}_{66}-\frac{\hat{\overline{Q}}_{13}\hat{\overline{Q}}_{23}}{\hat{\overline{Q}}_{33}}\right)\sum_{j=1}^{N}\overline{g}_{ij}\overline{u}_{rj} - \left(\frac{h}{R_m}\right)^2\frac{m}{\overline{r}_i^2}\left(\hat{\overline{Q}}_{22}+2\hat{\overline{Q}}_{66}-\frac{\hat{\overline{Q}}_{23}^2}{\hat{\overline{Q}}_{33}}\right)\overline{u}_{ri} - \left(\frac{h}{R_m}\right)^2\hat{\overline{Q}}_{66}\sum_{j=1}^{N}\overline{g}_{ij}^2\overline{u}_{\theta j} - \left(\frac{h}{R_m}\right)^2\frac{\hat{\overline{Q}}_{66}}{\overline{r}_i}\sum_{j=1}^{N}\overline{g}_{ij}\overline{u}_{\theta j} + \left(\frac{h}{R_m}\right)^2\frac{m^2}{\overline{r}_i^2}\left(\hat{\overline{Q}}_{22}-\frac{\hat{\overline{Q}}_{23}^2}{\hat{\overline{Q}}_{33}}\right)\overline{u}_{\theta i} + \left(\frac{h}{R_m}\right)^2\frac{2\hat{\overline{Q}}_{66}}{\overline{r}_i^2}\overline{u}_{\theta i} \tag{35f}$$

where

$$\begin{aligned} &\overline{\sigma}_{ki} = \overline{\sigma}_k(r,\theta,z),\ \ \overline{\tau}_{rzi} = \overline{\tau}_{rz}(r,\theta,z),\ \ \overline{\tau}_{\theta zi} = \overline{\tau}_{\theta z}(r,\theta,z),\\ &\overline{u}_{ki} = \overline{u}_k(r,\theta,z);\ \ (k = r_i,\theta,z) \end{aligned} \tag{36}$$

Substitution of Eqs. (22–23) into Eqs. (35a–f) results in the following state-space equations

$$\frac{\partial \bar{\boldsymbol{\delta}}_b}{\partial \bar{z}} = \bar{\mathbf{G}}_b\bar{\boldsymbol{\delta}}_b \tag{37}$$

in which $\bar{\boldsymbol{\delta}}_b = \left\{\ \overline{\sigma}_z\ \overline{u}_r\ \ \overline{u}_\theta\ \overline{u}_z\ \ \overline{\tau}_{rz}\ \overline{\tau}_{\theta z}\ \right\}^T$ is the column matrix of state variables and $\overline{\mathbf{G}}_b$ is defined in Appendix section, where subscript b in Eq. (37) denotes the state equation includes the boundary conditions.

G is presented in appendix section; the above equation is a typical first-order differential equation with a definite answer. It should be noted that the current material is laminate, so its properties are different in different layers in terms of thickness, so the G matrix has different properties in terms of different thicknesses. On the other hand, since the thickness changes, the first-order equation introduced will have variable coefficients that are difficult to solve. Therefore, in order to solve the problem, the object can be divided into several layers in terms of thickness, and in each layer, the thickness is constant and equal to its thickness to be able to solve the equations. Obviously, the more layers we consider, the more accurate the answer

to the problem can be. Therefore, by solving the equations and the boundary conditions of the problem, the values of the introduced states in different places can be calculated, and other quantitative plane stress quantities can be determined through them. Now, by using a layer-wise technique, $\overline{\mathbf{G}}_b$ is reduced to the constant matrix, and then, Eq. (37) can be solved analytically for N_t fictitious layer as the below

$$\boldsymbol{\delta}_k(\overline{z}) = \boldsymbol{\delta}_{ok} \exp\big(\overline{\mathbf{G}}_{bk}(\overline{z} - \overline{z}_{k-1})\big), \quad \overline{z}_{k-1} \le \overline{z} \le \overline{z}_k \tag{38}$$

At the inner and outer radius of kth layer, the relation between the state variables can be given as follows:

$$\boldsymbol{\delta}_\mathrm{k}(\overline{z}_\mathrm{k}) = \overline{\mathbf{M}}_\mathrm{k}\boldsymbol{\delta}_\mathrm{ok}, \tag{39}$$

in which $\overline{\mathbf{M}}_\mathrm{k} = \exp\left(\frac{\overline{\mathbf{G}}_\mathrm{bk}\overline{h}_\mathrm{f}}{N_\mathrm{t}}\right)$.

6 Various types of sandwich MHL composite circular/annular plates

6.1 Type-1 (two layers)

Similarly, state-space equations for Type-1 can be derived by using Eq. (39);

$$\frac{\partial\bar{\boldsymbol{\delta}}_{bi}}{\partial\overline{z}} = \overline{\mathbf{G}}_{bi}\bar{\boldsymbol{\delta}}_{bi} \quad \text{and}: i = (b, t) \tag{40}$$

By using the continuity of displacements, and equilibrium equation at each layers, the following relations between the inner, outer layers can be derived

$$\bar{\boldsymbol{\delta}}_{bo} = \overline{\mathbf{M}}_b\bar{\boldsymbol{\delta}}_{bi} \quad \overline{\mathbf{M}}_b = \prod_{k=Nt}^{1} \exp\left(\frac{\overline{\mathbf{G}}_{bk}\overline{h}_b}{N_t}\right) \tag{41a}$$

$$\bar{\boldsymbol{\delta}}_{to} = \overline{\mathbf{M}}_t\bar{\boldsymbol{\delta}}_{ti} \quad \overline{\mathbf{M}}_t = \prod_{k=Nt}^{1} \exp\left(\frac{\overline{\mathbf{G}}_{bk}\overline{h}_t}{N_t}\right) \tag{41b}$$

Using continuity of displacements and equilibrium equation at each layer and using Eqs. (41a–b) result in the following relation

$$\bar{\boldsymbol{\delta}}_\mathrm{to} = \mathbf{A}_\mathrm{bi} \tag{42}$$

where $\mathbf{A} = \overline{\mathbf{M}}_t\overline{\mathbf{M}}_b$.

6.2 Type-2 (three layers)

Similarly, state-space equations for Type-2 can be derived by using Eq. (39);

$$\frac{\partial\bar{\boldsymbol{\delta}}_{bi}}{\partial\overline{z}} = \overline{\mathbf{G}}_{bi}\bar{\boldsymbol{\delta}}_{bi} \quad \text{and}: i = (b, m, t) \tag{43}$$

By assuming the continuity of displacements, and equilibrium equation at each fictitious layer, we have:

$$\bar{\boldsymbol{\delta}}_{bo} = \overline{\mathbf{M}}_b\bar{\boldsymbol{\delta}}_{bi} \quad \overline{\mathbf{M}}_b = \prod_{k=Nt}^{1} \exp\left(\frac{\overline{\mathbf{G}}_{bk}\overline{h}_b}{N_t}\right) \tag{44a}$$

$$\bar{\boldsymbol{\delta}}_{mo} = \overline{\mathbf{M}}_m \bar{\boldsymbol{\delta}}_{mi} \quad \overline{\mathbf{M}}_m = \prod_{k=Nt}^{1} \exp\left(\frac{\overline{\mathbf{G}}_{bk}\overline{h}_m}{N_t}\right) \tag{44b}$$

$$\bar{\boldsymbol{\delta}}_{to} = \overline{\mathbf{M}}_t \bar{\boldsymbol{\delta}}_{ti} \quad \overline{\mathbf{M}}_t = \prod_{k=Nt}^{1} \exp\left(\frac{\overline{\mathbf{G}}_{bk}\overline{h}_t}{N_t}\right) \tag{44c}$$

By assuming continuity of displacements and equilibrium equation at each layer, and using Eq. (44a–c) results in the following relation, we have:

$$\bar{\boldsymbol{\delta}}_{to} = \mathbf{A}\bar{\boldsymbol{\delta}}_{bi} \tag{45}$$

where $\mathbf{A} = \overline{\mathbf{M}}_t\overline{\mathbf{M}}_m\overline{\mathbf{M}}_b$.

6.3 Type-3 (five layers)

Similarly, state-space equations for Type-3 can be derived by using Eq. (39):

$$\frac{\partial \bar{\boldsymbol{\delta}}_{\mathrm{bi}}}{\partial \overline{z}} = \bar{\mathbf{G}}_{bi}\bar{\boldsymbol{\delta}}_{bi} \quad \text{and} : i = (b, b_1, m, t_1, t) \tag{46}$$

By assuming continuity of displacements, and equilibrium equation at each layer, we have:

$$\bar{\boldsymbol{\delta}}_{bo} = \overline{\mathbf{M}}_b \bar{\boldsymbol{\delta}}_{bi} \quad \overline{\mathbf{M}}_b = \prod_{k=Nt}^{1} \exp\left(\frac{\overline{\mathbf{G}}_{bk}\overline{h}_b}{N_t}\right) \tag{47a}$$

$$\bar{\boldsymbol{\delta}}_{b_1o} = \overline{\mathbf{M}}_{b_1} \bar{\boldsymbol{\delta}}_{b_1i} \quad \overline{\mathbf{M}}_{b1} = \prod_{k=Nt}^{1} \exp\left(\frac{\overline{\mathbf{G}}_{bk}\overline{h}_{b_1}}{N_t}\right) \tag{47b}$$

$$\bar{\boldsymbol{\delta}}_{mo} = \overline{\mathbf{M}}_m \bar{\boldsymbol{\delta}}_{mi} \quad \overline{\mathbf{M}}_m = \prod_{k=Nt}^{1} \exp\left(\frac{\overline{\mathbf{G}}_{bk}\overline{h}_m}{N_t}\right) \tag{47c}$$

$$\bar{\boldsymbol{\delta}}_{t_1o} = \overline{\mathbf{M}}_{t_1} \bar{\boldsymbol{\delta}}_{t_1i} \quad \overline{\mathbf{M}}_{t_1} = \prod_{k=Nt}^{1} \exp\left(\frac{\overline{\mathbf{G}}_{bk}\overline{h}_{t_1}}{N_t}\right) \tag{47d}$$

$$\bar{\boldsymbol{\delta}}_{to} = \overline{\mathbf{M}}_t \bar{\boldsymbol{\delta}}_{ti} \quad \overline{\mathbf{M}}_t = \prod_{k=Nt}^{1} \exp\left(\frac{\overline{\mathbf{G}}_{bk}\overline{h}_t}{N_t}\right) \tag{47e}$$

By assuming the continuity of displacements and equilibrium equation at each layer, and using Eq. (47a–c) results in the following relation, we have:

$$\bar{\boldsymbol{\delta}}_{to} = \mathbf{A}\bar{\boldsymbol{\delta}}_{bi} \tag{48}$$

where $\mathbf{A} = \mathbf{M}_t\mathbf{M}_{t_1}\mathbf{M}_m\mathbf{M}_{b_1}\mathbf{M}_b$.

6.4 Type-4 (seven layers)

Similarly, state-space equations for Type-4 can be derived by using Eq. (39):

$$\frac{\partial \bar{\boldsymbol{\delta}}_{bi}}{\partial \overline{z}} = \overline{\mathbf{G}}_{bi}\bar{\boldsymbol{\delta}}_{bi} \quad \text{and} : i = (b, b_1, b_2, m, t_2, t_1, t) \tag{49}$$

As the repeat process, like three and five layers, we have:

$$\bar{\boldsymbol{\delta}}_{bo} = \overline{\mathbf{M}}_b \bar{\boldsymbol{\delta}}_{bi} \qquad \mathbf{M}_b = \prod_{k=Nt}^{1} \exp\left(\frac{\overline{\mathbf{G}}_{bk}\overline{h}_b}{N_t}\right) \tag{50a}$$

$$\bar{\boldsymbol{\delta}}_{b_1 o} = \overline{\mathbf{M}}_{b_1} \bar{\boldsymbol{\delta}}_{b_1 i} \qquad \mathbf{M}_{b1} = \prod_{k=Nt}^{1} \exp\left(\frac{\overline{\mathbf{G}}_{bk}\overline{h}_{b_1}}{N_t}\right) \tag{50b}$$

$$\bar{\boldsymbol{\delta}}_{b_2 o} = \overline{\mathbf{M}}_{b_2} \bar{\boldsymbol{\delta}}_{b_2 i} \qquad \mathbf{M}_{b2} = \prod_{k=Nt}^{1} \exp\left(\frac{\overline{\mathbf{G}}_{bk}\overline{h}_{b_2}}{N_t}\right) \tag{50c}$$

$$\bar{\boldsymbol{\delta}}_{mo} = \overline{\mathbf{M}}_m \bar{\boldsymbol{\delta}}_{mi} \qquad \mathbf{M}_m = \prod_{k=Nt}^{1} \exp\left(\frac{\overline{\mathbf{G}}_{bk}\overline{h}_m}{N_t}\right) \tag{50d}$$

$$\bar{\boldsymbol{\delta}}_{t_2 o} = \overline{\mathbf{M}}_{t_2} \bar{\boldsymbol{\delta}}_{t_2 i} \qquad \mathbf{M}_{t_2} = \prod_{k=Nt}^{1} \exp\left(\frac{\overline{\mathbf{G}}_{bk}\overline{h}_{t_2}}{N_t}\right) \tag{50e}$$

$$\bar{\boldsymbol{\delta}}_{t_1 o} = \overline{\mathbf{M}}_{t_1} \bar{\boldsymbol{\delta}}_{t_1 i} \qquad \mathbf{M}_{t_1} = \prod_{k=Nt}^{1} \exp\left(\frac{\overline{\mathbf{G}}_{bk}\overline{h}_{t_1}}{N_t}\right) \tag{50f}$$

$$\bar{\boldsymbol{\delta}}_{to} = \overline{\mathbf{M}}_t \bar{\boldsymbol{\delta}}_{ti} \qquad \mathbf{M}_t = \prod_{k=Nt}^{1} \exp\left(\frac{\overline{\mathbf{G}}_{bk}\overline{h}_t}{N_t}\right) \tag{50g}$$

By assuming continuity of displacements, and equilibrium equation at each fictitious layers, we have:

$$\bar{\boldsymbol{\delta}}_{to} = \mathbf{A}\bar{\boldsymbol{\delta}}_{bi} \tag{51}$$

where $\mathbf{A} = \mathbf{M}_t\mathbf{M}_{t1}\mathbf{M}_{t2}\mathbf{M}_m\mathbf{M}_{b2}\mathbf{M}_{b1}\mathbf{M}_b$.

7 Static analysis

For static analysis, it is assumed the following surface traction boundary condition.

$$\begin{aligned} &\overline{\sigma}_z = \Im, \quad \overline{\tau}_{rz} = 0, \quad \overline{\tau}_{\theta z} = \Im_r \qquad \text{at } \ \overline{z} = -\frac{1}{2} \\ &\overline{\sigma}_z = \overline{p}\cos(\theta_0), \quad \overline{\tau}_{rz} = \overline{\tau}_{\theta z} = 0 \qquad \text{at } \ \overline{z} = \frac{1}{2} \end{aligned} \tag{52}$$

Applying Eq. (51) into Eqs. (42), (45), (48), and (51) leads to the following nonhomogeneous equation:

$$\begin{bmatrix} A_{12} & A_{13} + A_{16}\Im_r & A_{14} + A_{11}\Im \\ A_{52} & A_{53} + A_{56}\Im_r & A_{54} + A_{51}\Im \\ A_{62} & A_{53} + A_{56}\Im_r & A_{64} + A_{61}\Im \end{bmatrix} \begin{Bmatrix} \overline{u}_r \\ \overline{u}_\theta \\ \overline{u}_z \end{Bmatrix}_{\overline{z}=-\frac{1}{2}} = \begin{Bmatrix} \overline{p}\cos(\theta_0) \\ 0 \\ 0 \end{Bmatrix}_{\overline{z}=\frac{1}{2}} \tag{53}$$

where $\overline{p} = \{\overline{p}_1, \ldots\ldots, \overline{p}_N\}^T$. Displacements at the bottom surface are computed by solving Eq. (53), and then, by using Eqs. (42, 45, 48, 51) transverse normal and shear stresses, as

well as displacements as a function of radial coordination, are determined. Finally, in-plane normal and shear stresses are computed from the following equations:

$$\bar{\sigma}_{ri} = \frac{\hat{\bar{Q}}_{13}}{\hat{\bar{Q}}_{33}}\bar{\sigma}_{zi} + \frac{h}{R_m}\left(\hat{\bar{Q}}_{11} - \frac{\hat{\bar{Q}}_{13}^2}{\hat{\bar{Q}}_{33}}\right)\sum_{j=1}^{N}\bar{g}_{ij}\bar{u}_{rj} + \frac{h}{R_m}\frac{1}{\bar{r}_i}\left(\hat{\bar{Q}}_{12} - \frac{\hat{\bar{Q}}_{13}\hat{\bar{Q}}_{23}}{\hat{\bar{Q}}_{33}}\right)(\bar{u}_{ri} - m\bar{u}_{\theta i}) \tag{54a}$$

$$\bar{\sigma}_{\theta i} = \frac{\hat{\bar{Q}}_{23}}{\hat{\bar{Q}}_{33}}\bar{\sigma}_{zi} + \frac{h}{R_m}\left(\hat{\bar{Q}}_{12} - \frac{\hat{\bar{Q}}_{13}\hat{\bar{Q}}_{23}}{\hat{\bar{Q}}_{33}}\right)\sum_{j=1}^{N}\bar{g}_{ij}\bar{u}_{rj} + \frac{h}{R_m}\frac{1}{\bar{r}_i}\left(\hat{\bar{Q}}_{22} - \frac{\hat{\bar{Q}}_{23}^2}{\hat{\bar{Q}}_{33}}\right)(\bar{u}_{ri} - m\bar{u}_{\theta i}) \tag{54b}$$

$$\overline{\tau}_{r\theta i} = \frac{h}{R_m}\frac{m}{r_i}\hat{\bar{Q}}_{66}u_{ri} + \frac{h}{R_m}\hat{\bar{Q}}_{66}\sum_{j=1}^{N}\overline{g}_{ij}\overline{u}_{\theta j} + \frac{h}{R_m}\frac{\hat{\bar{Q}}_{66}}{\overline{r}_i}\overline{u}_{\theta i} \tag{54c}$$

8 Numerical results and discussion

Subsequently, we present a comprehensive parameter study to quantify the effects of various parameters on the bending response of MHLNCAAP/MHLNCACP. The geometrical and material characteristics of constituent materials are found in Table 1.

8.1 Validation

The properties in this validation section can be written as:

$$E(z) = E_m\left(\frac{h-2z}{2h}\right)^n + E_c\left[1 - \left(\frac{h-2z}{2h}\right)^n\right] \tag{55a}$$

$$E_{\mathrm{r}} = 0.396,\ E_{\mathrm{c}} = 125.83 \times 10^9,\ E_{\mathrm{m}} = E_{\mathrm{c}} \times E_{\mathrm{r}} \tag{55b}$$

$$R_{\mathrm{o}} = 1,\ h = 0.2R_{\mathrm{o}}, n = 0.288 \tag{55c}$$

Table 1 The properties of MHLNC [81] and poroelastic constant [82]

Carbon (fiber)	Epoxy (matrix)	Carbon nanotube	Poroelastic constants
$E_{11}^f(\mathrm{GPa}) = 233.05$	$v^m = 0.34$	$E^{\mathrm{cnt}}(\mathrm{Gpa}) = 640$	$\gamma = 0.27$
$E_{22}^f(\mathrm{GPa}) = 23.1$	$\rho^{\mathrm{m}}\left(\frac{\mathrm{kg}}{\mathrm{m}^3}\right) = 1200$	$D^{\mathrm{cnt}}(m) = 0.14 \times 10^{-9}$	$k_{\mathrm{u}} = 41[\mathrm{Gpa}]$
$G_{11}^f(\mathrm{GPa}) = 8.96$	$E^{\mathrm{m}}(\mathrm{Gpa}) = 3.51$	$T^{\mathrm{cnt}}(m) = 0.034 \times 10^{-9}$	$k = 35$ [Gpa]
$\upsilon^f = 0.2$		$L^{\mathrm{cnt}}(m) = 0.25 \times 10^{-9}$	$k_{\mathrm{f}} = 3.3[\mathrm{Kpa}]$
$\rho^f\left(\frac{\mathrm{kg}}{\mathrm{m}^3}\right) = 1750$		$v_{12} = 0.33$	$\emptyset = 0.02$
		$\rho^{\mathrm{cnt}}\left(kg/m^3\right) = 1350$	

Table 2 Comparison the $\overline{w}_0^F(0,0)$ of functionally graded clamped circular plates with the results in Ref. [83]

n	h/a = 0.05		h/a = 0.1		h/a = 0.15		h/a = 0.2	
	Ref. [83]	P.S	Ref. [83]	P.S	Ref. [83]	P.S	Ref. [83]	P.S
0	2.554	2.8702	2.639	2.9195	2.781	3.1057	2.979	3.2186
2	1.402	1.5820	1.444	1.6081	1.515	1.6962	1.613	1.8903
4	1.282	1.4483	1.320	1.4727	1.384	1.5513	1.473	1.6545
6	1.220	1.3796	1.257	1.4037	1.318	1.4792	I.404	1.5656
8	1.181	1.3366	1.217	1.3605	I.278	1.4348	1.362	1.5625
10	1.155	1.3070	1.190	1.3307	1.250	1.4043	I.333	1.5641
15	1.114	1.2621	1.149	1.2853	1.208	1.3584	1.289	1.4750
20	I.092	1.2369	1.126	1.2597	1.184	1.3326	I.265	1.3996
25	1.077	1.2208	1.112	1.2433	1.169	1.3162	1.250	1.4209
30	1.067	1.2096	1.101	1.2319	1.159	1.3047	1.239	1.3555
35	1.060	1.2014	1.094	1.2235	1.151	1.2964	1.231	1.3583
40	1.054	1.1952	1.088	1.2170	1.145	1.2900	1.225	1.4598
50	1.046	1.1903	1.080	1.2119	1.137	1.2850	1.216	1.3685
10^2	1.029	1.1863	1.063	1.2078	1.119	1.2810	1.199	1.3925
10^3	1.013	1.1683	1.047	1.1892	1.103	1.2624	1.182	1.3448
10^4	1.011	1.1569	1.045	1.1773	1.101	1.2508	1.180	1.3012
10^5	1.011	1.1569	1.045	1.1773	1.101	1.2508	1.180	1.3880

In Eq. (55a), n shows the FG power index. The dimensionless form of stress and displacement in this example can be written as:

$$\bar{w}_0^F = \frac{64 w_0^F D_c}{q_0 R_o^4} = \frac{D_c}{\Omega_1}\left[1-\left(\frac{r}{R_o}\right)^2\right]^2 + \frac{8}{3K_s^2(1-v_c)}\left(\frac{h}{R_o}\right)^2\left[1-\left(\frac{r}{R_o}\right)^2\right]\left(\frac{1+n}{E_r+n}\right) \tag{56a}$$

$$\bar{u}_0^F = \frac{64 u_0^F D_c}{q_0 R_o^4} = \frac{D_c}{\Omega_1}\left[1-\left(\frac{r}{R_o}\right)^2\right]^2 + \frac{8}{3K_s^2(1-v_c)}\left(\frac{h}{R_o}\right)^2\left[1-\left(\frac{r}{R_o}\right)^2\right]\left(\frac{1+n}{E_r+n}\right) \tag{56b}$$

$$\left(\overline{\sigma}_0^F, \overline{\tau}_{rz}^F\right) = \left(\frac{\sigma_0^F}{q_0}, \frac{\tau_{rz}^F}{q_0}\right) \tag{56c}$$

Table 2 presents a validation study for proving the result of the current paper. In this regard, the non-dimensional maximum deflections in the conditions of various FG power index (n) value,$\overline{w}_0^F(0,0)$ are compared with those outcomes in Ref. [83]. As shown in the comparison studies, the results of this paper have a suitable agreement with the presented study in the literature. As can be seen, there is good agreement between the results.

For another verification for this work, according to Table 3, it is revealed that the proposed modeling can provide good agreement with Ref. [84] where the influences of compatibility

Table 3 Compare the maximum deflections (m) of axisymmetric plates made of various materials with the result in Ref. [84]

	Circular plate		Annular plate	
	Ref. [84]	P.S	Ref. [84]	P.S
Polyimide	2.626×10^{-3}	2.6342×10^{-3}	0.2720×10^{-3}	0.2727×10^{-3}
1% CNT-RP	2.284×10^{-3}	2.2913×10^{-3}	0.2365×10^{-3}	0.2372×10^{-3}
3% CNT-RP	1.720×10^{-3}	1.7285×10^{-3}	0.1782×10^{-3}	0.1787×10^{-3}
5% CNT-RP	1.397×10^{-3}	1.4002×10^{-3}	0.1446×10^{-3}	0.1451×10^{-3}
5% CF-RP	2.309×10^{-3}	2.3151×10^{-3}	0.2391×10^{-3}	0.2398×10^{-3}
10% CF-RP	2.076×10^{-3}	2.0810×10^{-3}	0.2149×10^{-3}	0.2156×10^{-3}
20% CF-RP	1.606×10^{-3}	1.6129×10^{-3}	0.1663×10^{-3}	0.1668×10^{-3}
0.95% CNT–5% CF-RP	2.012×10^{-3}	2.0195×10^{-3}	0.2083×10^{-3}	0.2089×10^{-3}
2.85% CNT–5% CF-RP	1.523×10^{-3}	1.5387×10^{-3}	0.1577×10^{-3}	0.1582×10^{-3}
4.75% CNT–5% CF-RP	1.242×10^{-3}	1.2741×10^{-3}	0.1286×10^{-3}	0.1292×10^{-3}
0.9% CNT–10% CF-RP	1.811×10^{-3}	1.8210×10^{-3}	0.1876×10^{-3}	0.1881×10^{-3}
2.7% CNT–10% CF-RP	1.376×10^{-3}	1.3812×10^{-3}	0.1425×10^{-3}	0.1431×10^{-3}
4.5% CNT–10% CF-RP	1.126×10^{-3}	1.1314×10^{-3}	0.1166×10^{-3}	0.1169×10^{-3}
0.8% CNT–20% CF-RP	1.409×10^{-3}	1.4152×10^{-3}	0.1459×10^{-3}	0.1464×10^{-3}
2.4% CNT–20% CF-RP	1.085×10^{-3}	1.0916×10^{-3}	0.1124×10^{-3}	0.1127×10^{-3}
4% CNT–20% CF-RP	0.898×10^{-3}	0.9014×10^{-3}	0.0930×10^{-3}	0.0932×10^{-3}

Annular plate: $R_{\mathrm{i}} = 10\,\mathrm{mm}$, $R_o = 25mm$, $h = 10\,\mathrm{mm}$
Circular plate: $R_{\mathrm{o}} = 25\,\mathrm{mm}$, $h = 10\,\mathrm{mm}$
$P = 10^8$ [N/m^2]

conditions are ignored. As shown in Table 3, by increasing the CNT's volume fraction, the maximum deflection of the axisymmetric circular/annular plates decreases.

The influence of the node number (N) on the convergence condition is reported in Fig. 3 for the investigation of bending response and stress analysis of the laminated disk. As a general result, there is a break in the diagram of stress fields. In this regard, the bending behaviors of the laminated structure with [0°/90°/0°] are presented for three values of N parameter. Based on the presented diagram in Fig. 3, we can report that when N is longer than seven, the stress and displacement fields don't have a dependency to N, so the convergence condition of the DQ method is achieved by employing seven grid points for the semi-analytical method. As a general result, there is a break in the diagram of stress fields.

The reason for the mentioned matter is that the mechanical properties of the layers are different, and the layer-wise technique is employed in the presented model (according to Eq. (42) for three layer's continuity).

The bending behaviors of the laminated annular plate are presented in Fig. 4 by having more attention to the effect of three kinds of boundary conditions. According to Fig. 4 when the structure is encountered with the clamped edges, the better bending response and the lowest stress are seen in the laminated structure. The meaning of better bending response is that the structure with lower magnitude stress and displacement fields has a better bending response in compassion with other ones. In addition, if the structure encounters the clamped edges (C–C and C–S boundary conditions), we cannot find a remarkable change in the

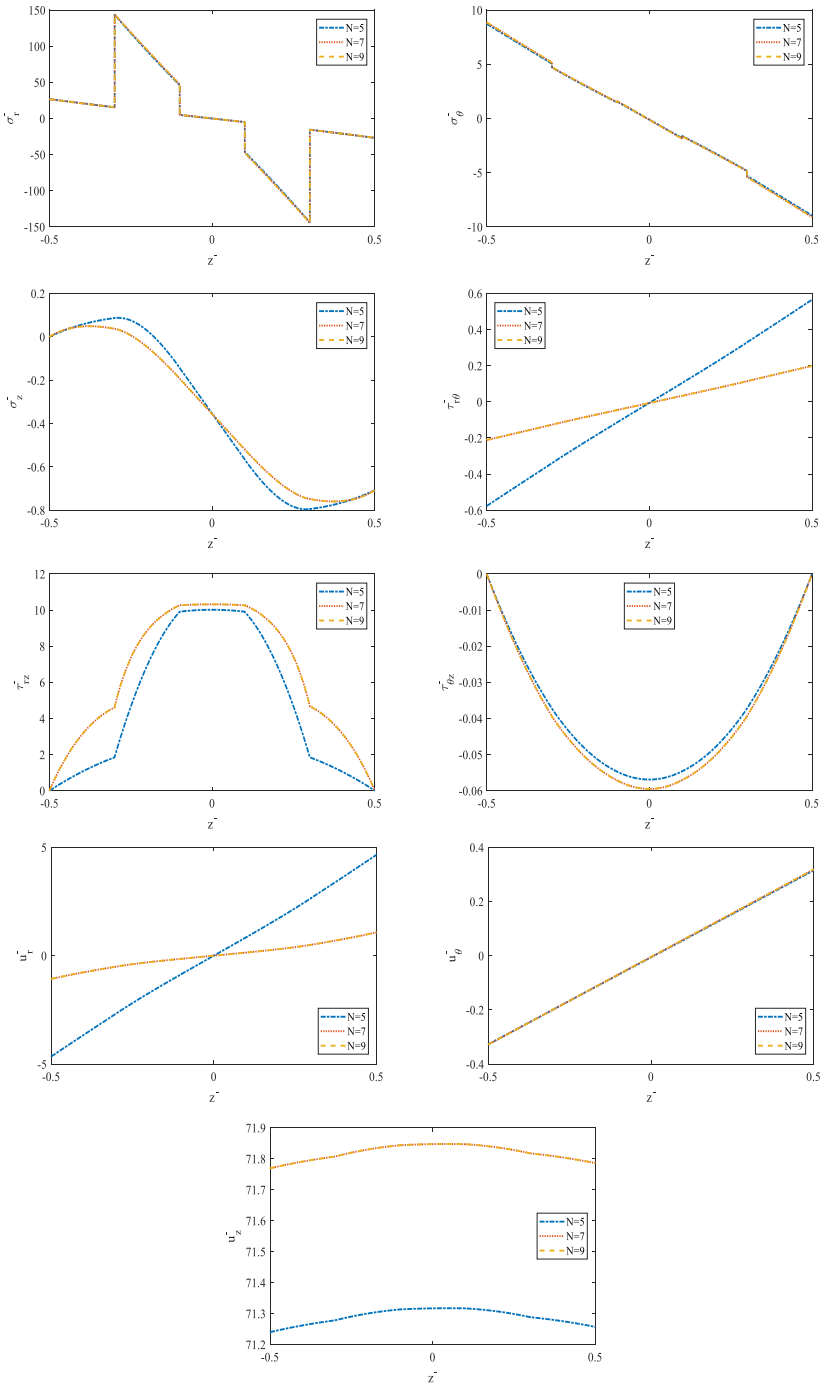

Fig. 3 Stress and displacement fields of the laminated structure for three N in the DQ method with $R_o/R_i = 1.2$, $h = 0.01R_i$, $W_{CNT} = 0.02$, $V_F = 0.8$, $[90^0/0^0/90^0/0^0/90^0]$, $K_{wo} = K_{po} = 100$, $f_1 = f_2 = P_1 = P_2 = 0.1$, $K_{r10} = K_{r20} = 100$, $\theta_o = \pi/4$, clamped–clamped boundary conditions, and MHLNCAP

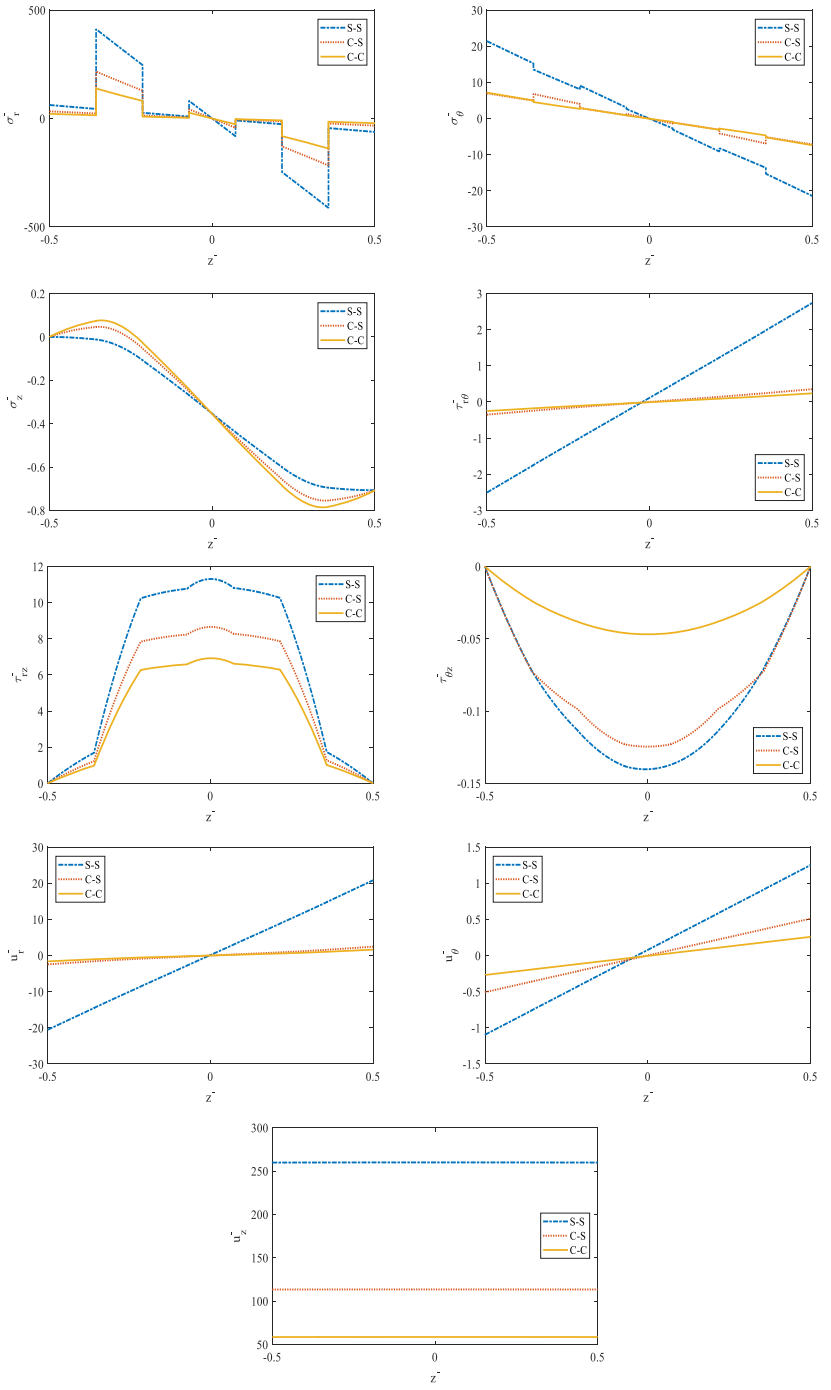

Fig. 4 Effect of three kinds of boundary conditions stress and displacement fields of the laminated structure with $R_o/R_i = 1.2$, $h = 0.01R_i$, $W_{CNT} = 0.02$, $V_F = 0.8$, [90°/0°/90°/0°/90°/0°/90°], $K_{wo} = K_{po} = 100$, $f_1 = f_2 = P_1 = P_2 = 0.1$, $K_{r10} = K_{r20} = 100$, and MHLNCAP

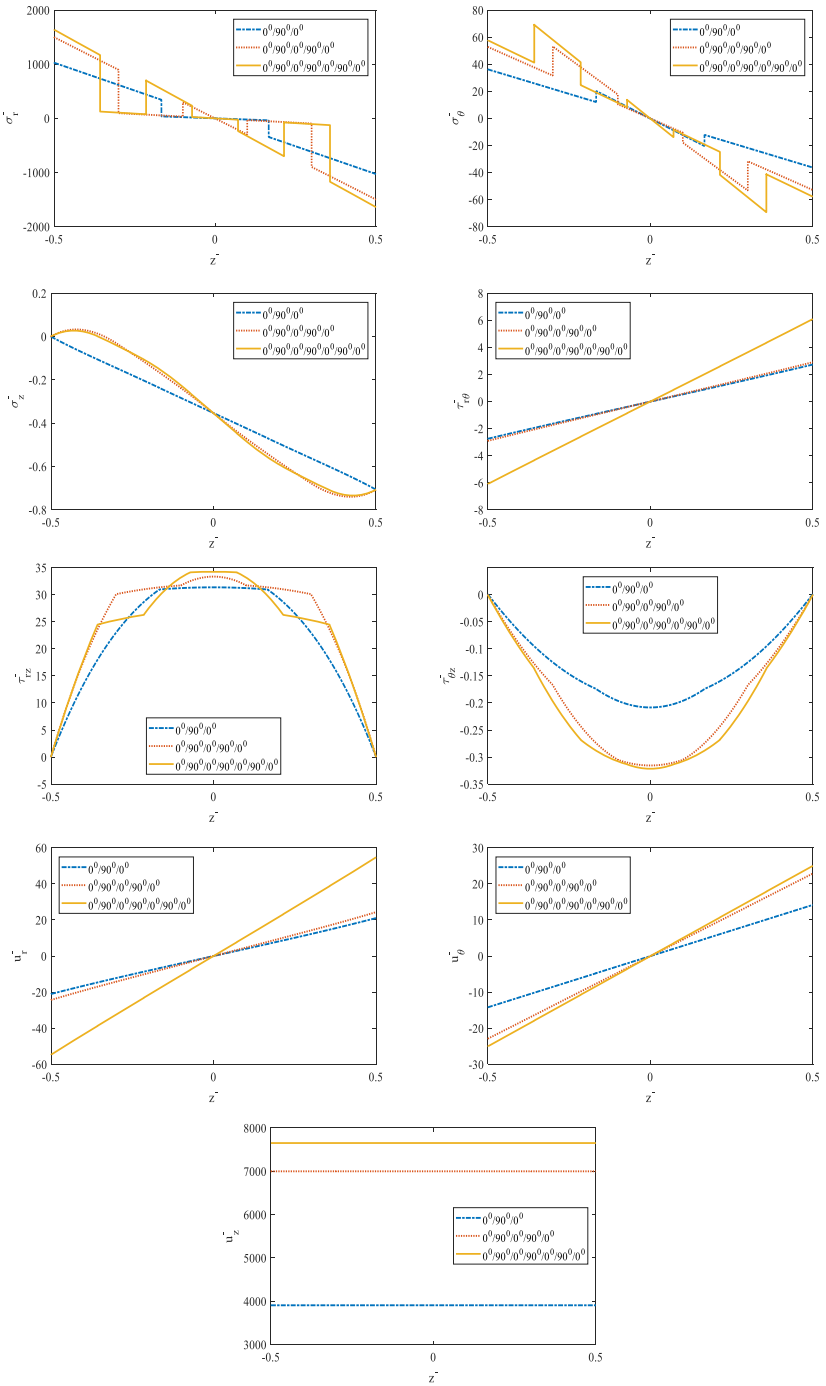

Fig. 5 Stress and displacement fields of the laminated structure for three number of layers with $R_o/R_i = 1.5$, $h = 0.01R_i$, $W_{CNT} = 0.02$, $V_F = 0.8$, $K_{wo} = K_{po} = 100, f_1 = f_2 = P_1 = P_2 = 0.1$, $K_{r10} = K_{r20} = 100$, clamped–clamped boundary conditions, and MHLNCAP

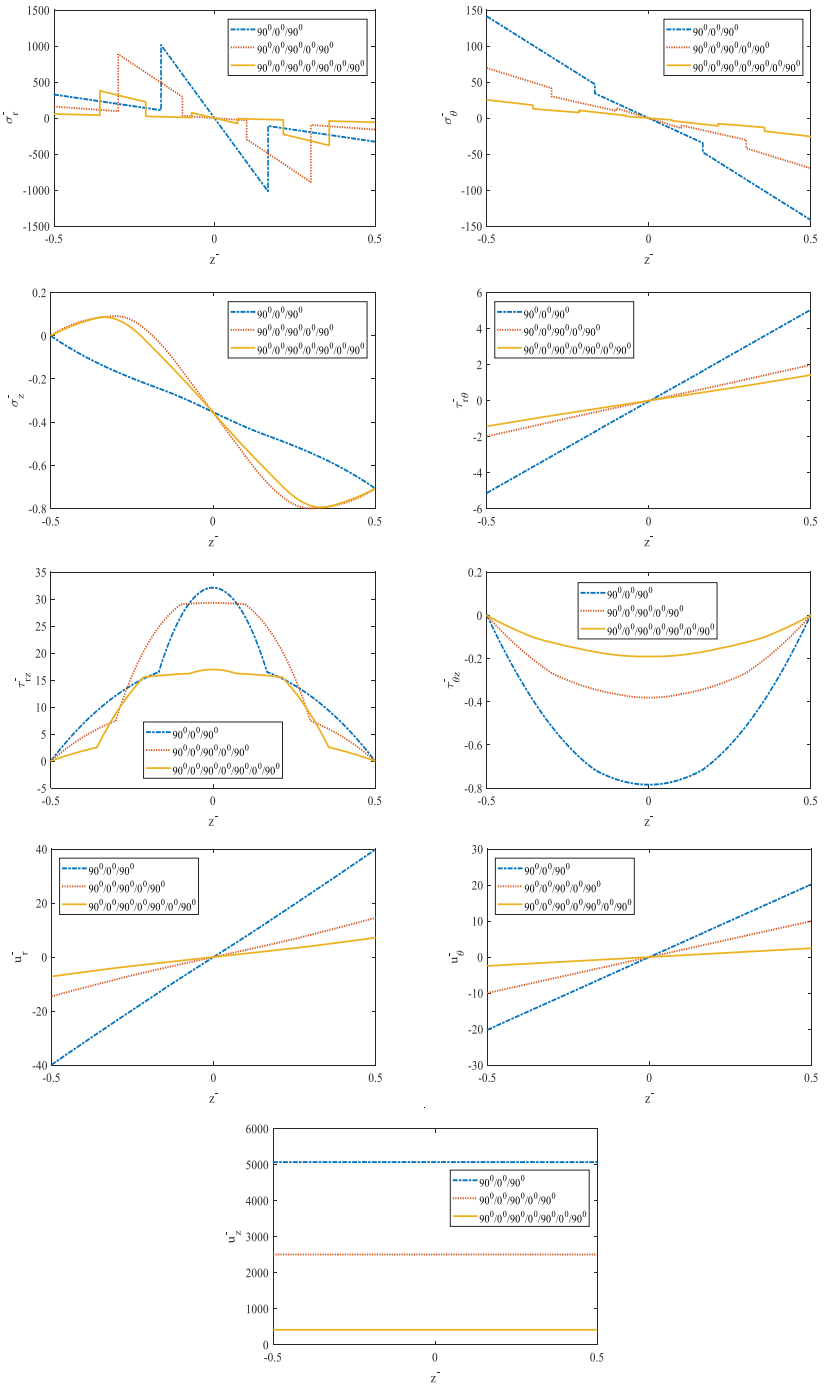

Fig. 6 Stress and displacement fields of the laminated structure for three number of layers with $R_o/R_i = 1.5$, $h = 0.01R_i$, $W_{CNT} = 0.02$, $V_F = 0.8$, $K_{wo} = K_{po} = 100, f_1 = f_2 = P_1 = P_2 = 0.1$, $K_{r10} = K_{r20} = 100$, clamped–clamped boundary conditions, and MHLNCAP

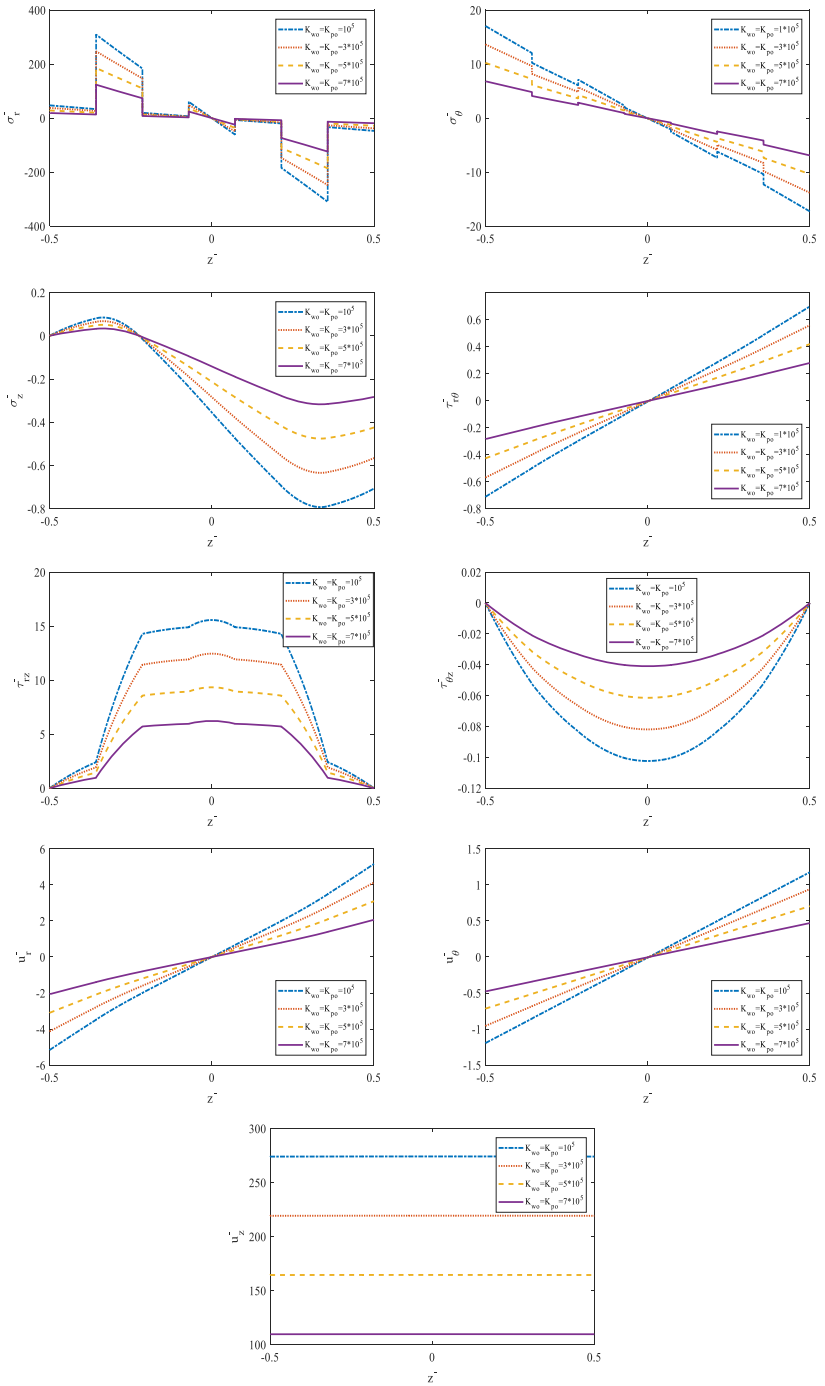

Fig. 7 Stress and displacement fields of the laminated structure for Effect of the foundation coefficients with $R_o/R_i = 1.3$, $h = 0.01R_i$, $W_{CNT} = 0.02$, $V_F = 0.8$, [90°/0°/90°/0°/90°/0°/90°], $f_1 = f_2 = P_1 = P_2 = 0.1$, $K_{r10} = K_{r20} = 100$, $\theta_o = \pi/4$, clamped–clamped boundary conditions, and MHLNCAP

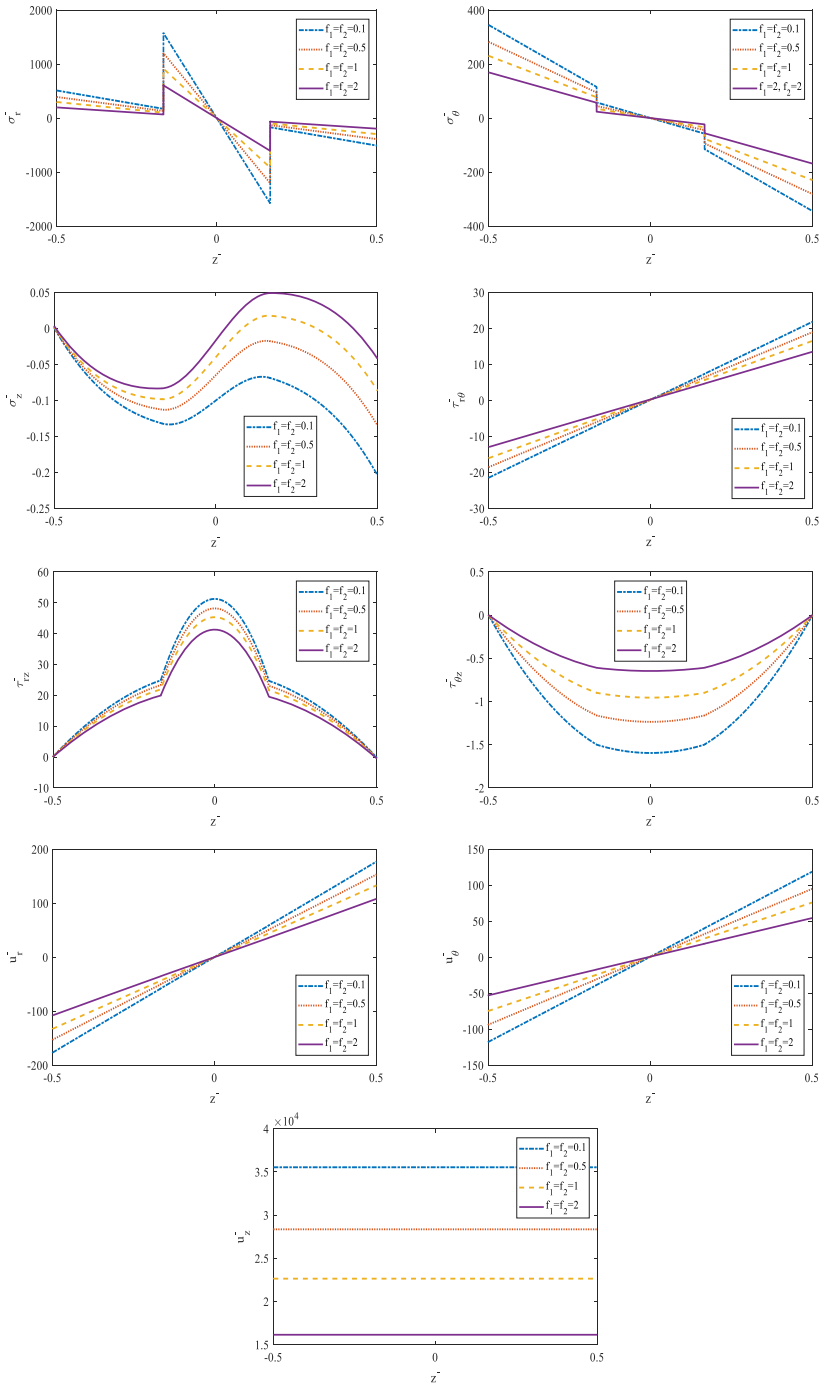

Fig. 8 Effect of foundation gradient index on the stress and displacement fields of the laminated structure with $R_o/R_i = 2$, $h = 0.01R_i$, $W_{CNT} = 0.02$, $V_F = 0.8$, [90°/0°/90°], $K_{wo} = K_{po} = 5 \times 10^4$, $K_{r10} = K_{r20} = 100$, $\theta_o = \pi/4$, $P_1 = P_2 = 0.1$, clamped–clamped boundary conditions, and annular plate

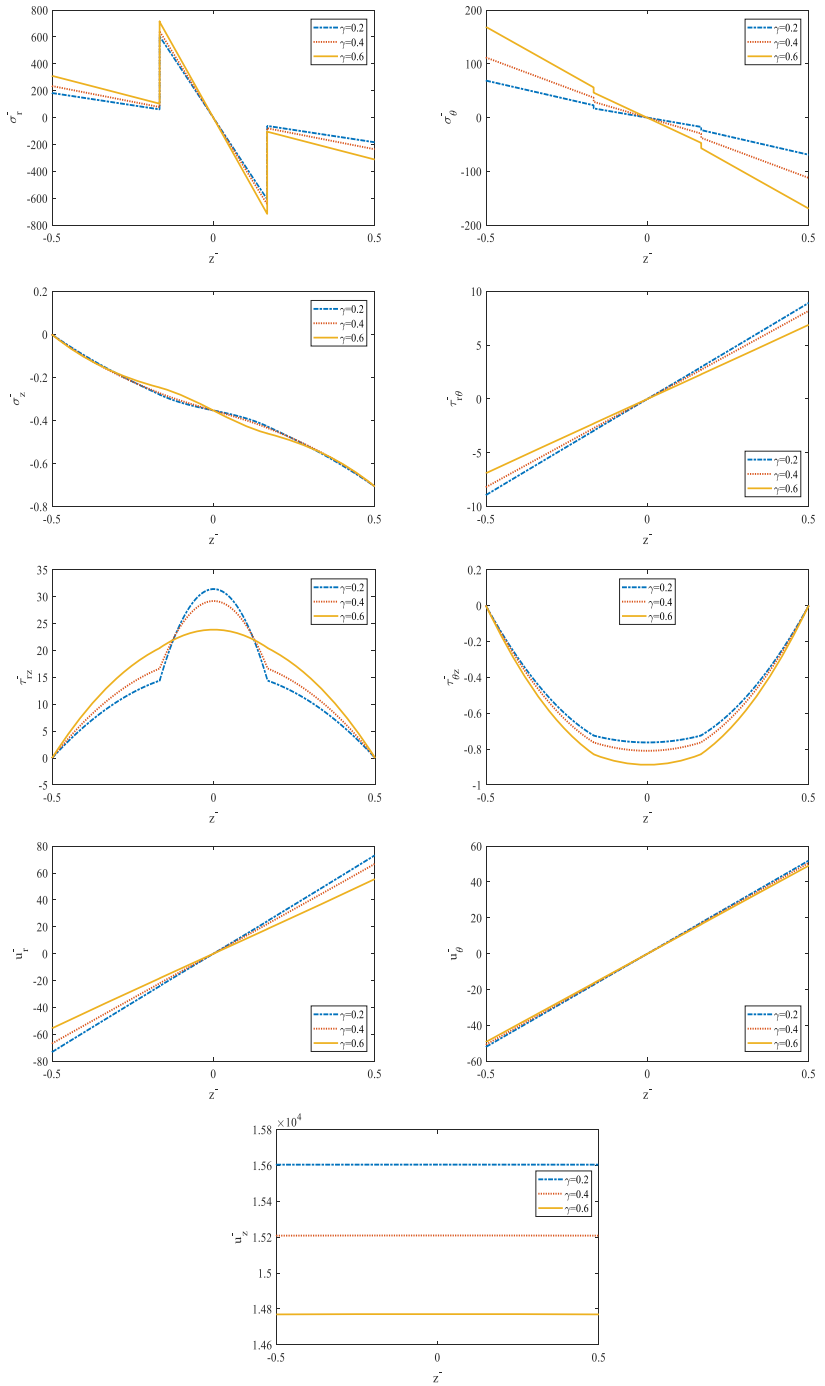

Fig. 9 Effect of Biot's coefficient on the stress and displacement fields of the laminated structure with $R_o/R_i = 2$, $h = 0.01R_i$, $W_{CNT} = 0.02$, $V_F = 0.8$, [90°/0°/90°/0°/90°/0°/90°], $K_{wo} = K_{po} = 100$, $K_{r10} = K_{r20} = 100$, $\theta_o = \pi/4, f_1 = f_2 = P_1 = P_2 = 0.1$, clamped–clamped boundary conditions, and MHLNCAP

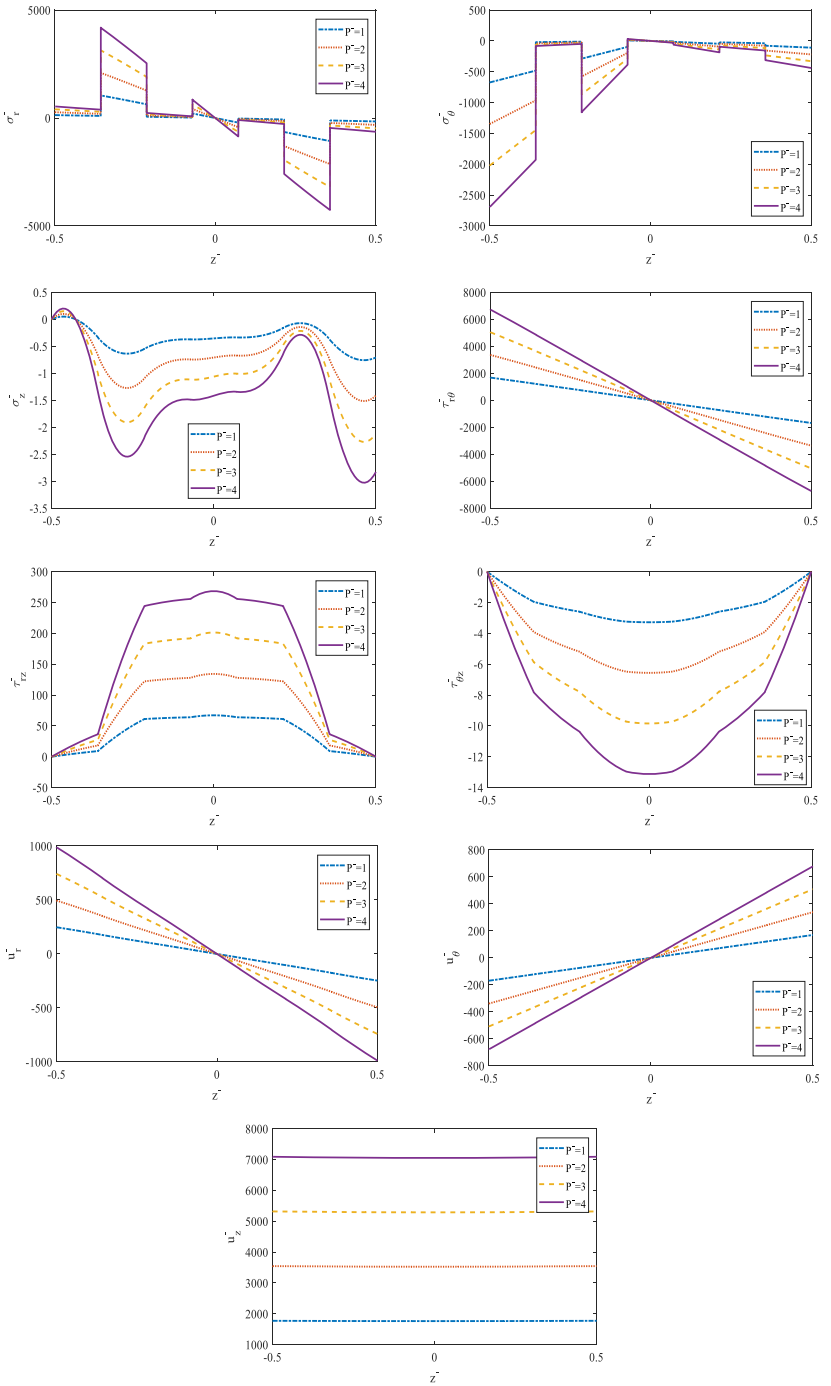

Fig. 10 Effect of external pressure on the stress and displacement fields of the laminated structure with $h = 0.01\mathrm{R_o}$, $W_{\mathrm{CNT}} = 0.02$, $V_{\mathrm{F}} = 0.8$, [90°/0°/90°/0°/90°/0°/90°], $K_{\mathrm{wo}} = K_{\mathrm{po}} = 100$, $K_{\mathrm{r10}} = K_{\mathrm{r20}} = 100$, $\theta_{\mathrm{o}} = \pi/4, f_1 = f_2 = P_1 = P_2 = 0.1$, hinged–clamped boundary conditions, and MHLNCCP

radial bending response, but by having simply–simply edges, we can see an increase in the radial displacement field. Also, in the middle layers we cannot see any effect from boundary conditions on the normal axial stress, while in the inner and outer layers, when the structure is encountered with simple edges, we can see the highest axial normal stress. Also, the impact of boundary conditions on normal stress is more remarkable in the inner and outer layers. Besides, for each boundary condition, the maximum shear stress is seen in the middle layers, and the structure with clamped edges has the lowest shear stress along the thickness direction. Last but not the list, there is a fluctuation in the diagram of $\overline{\sigma}_{\mathrm{r}}$, $\overline{\sigma}_{\theta}$, and $\overline{\tau}_{\mathrm{rz}}$ and the intensity of the fluctuation decreases by increasing the rigidity of the boundary conditions. In other words, when the structure is fixed with more rigid boundary conditions, the sensitivity of the static response to the layers' characteristics decreases. The reason for the mentioned fluctuation is that the mechanical properties of the layers are different, and the layer-wise technique is employed in the presented model.

Figures 5 and 6 present the effects of the number of layers and two kinds of laminate patterns (horizontal pattern [0°/90°.] and vertical pattern [90°/0°]) on the stress analysis and bending behaviors of the structure. With respect to the diagrams of Figs. 5 and 6, we can see that there are fluctuations in the diagram of $\overline{\sigma}_{\mathrm{r}}$, $\overline{\sigma}_{\theta}$, and $\overline{\tau}_{\mathrm{rz}}$ and the intensity and number of the fluctuations decrease by increasing the number of layers in the laminated disk with a vertical pattern. In contrast, by increasing the number of layers in the horizontal pattern, the fluctuations increase. Accordingly, for horizontal laminate pattern, as the number of layer increases, stress and displacement fields increase, so the bending behaviors of the system become weak. In contrast, when the structure is made by a vertical laminate pattern by increasing the number of layers the stress and displacement fields decrease, the bending responses of the laminated system improve. In conclusion, in this section, increasing the number of layers is a reason to improve bending responses, but this is only true for the vertical laminate pattern, while increasing the number of layers in the horizontal laminate pattern makes a negative impact on the static responses of the structure.

The purpose of Fig. 7 is an investigation about the effect of Winkler and Pasternak factors (K_{wo} and K_{po}) on the stress and displacement fields of the structure with [90°/0°/90°/0°/90°/0°/90°]. Accordingly, as the Winkler and Pasternak factors of the foundation increase, the in-plane and out-plane stress decreases. In addition, increasing the foundation factors is a reason to decrease the axial stress (σ_{z}) and this issue becomes bold by increasing z^{-} or at the outer layers. Also, the impact of Winkler and Pasternak factors on the in-plane or shear stress (τ_{rz} and $\tau_{\theta z}$) is more remarkable at the middle layers ($-0.4 \leq z^{-} \leq 0.1$). Last but not the list, there is a fluctuation in the diagram of $\overline{\sigma}_{\mathrm{r}}$, $\overline{\sigma}_{\theta}$, and $\overline{\tau}_{\mathrm{rz}}$ and the intensity of the fluctuation decreases by increasing Winkler and Pasternak factors. In other words, when the foundation becomes intense, the sensitivity of the static response to the layers' characteristics decreases. The reason for the mentioned fluctuation is that the mechanical properties of the layers are different, and the layer-wise technique is employed in the presented model. Furthermore, the bending behavior of the laminated system improves due to increasing the value of Winkler and Pasternak factors, and stress distribution becomes more uniform.

The effect of foundation gradient parameters (f_1 and f_2) on the bending or static information of the laminated circular plate is explored in Fig. 8. Accordingly, increasing the foundation gradient parameters is a reason for improving the static responses of the system. As an important result, by increasing z^{-} the impact of the gradient factor of the foundation on the axial stress is intensified, and in the middle layers, the effect of gradient factor on the τ_{rz} and $\tau_{\theta z}$ increases. Also, the given information in Fig. 8 proves that the distribution of

the stress and displacement fields becomes more uniform by improving the foundation via increasing the gradient factor of the foundation.

The effect of the Biot's coefficient (γ) on the stress and displacement fields of the laminated structure is presented via the given diagram in Fig. 9. The presented diagram in this section shows that the Biot's coefficient makes a direct impact on radial and hoop stress. Along with the thickness, the impact of γ factor on the value of axial stress changes from direct to indirect for two times. Also, bending in the system decreases due to the increasing Biot's coefficient. Furthermore, the distribution of the stress and displacement fields becomes more uniform due to increasing the Biot's coefficient. Finally, static stability and bending behaviors of the system improve owing to increase the γ factor.

The impact of external pressure ($\overline{p}$) on the bending or static information of the laminated circular plate is explored in Fig. 10. According to Fig. 10, with each increase in the external pressure, the value of normal axial stress along with the thickness of the composite disk increases, and the mentioned relation is more considerable at the bigger value of $\overline{z}$. In addition, the sensitivity of the static response to the layers' characteristics is intensified by increasing the value of external pressure. Also, for each $\overline{z}$, as the external pressure increases, the stress and displacement fields increase. Furthermore, the impact of external pressure on the hoop shear stress, radial stress, and radial shear stress of the laminated circular plate becomes more considerable in the middle layers. In contrast, the impact of external pressure on normal hoop stress is considerable at the top and bottom layers. Finally, as $\overline{z}$ increases, the impact of external pursues on the axial stress reinforces.

Table 4 is presented for having an investigation about the impacts of the number of layers and poroelastic factor (K^p) on the bending behaviors of the laminated disk. Accordingly, K^p factor and number of laminated layers have a positive effect on the bending behaviors of the system, so the displacement fields increase, and stress fields decrease.

Figure 11 presents to study the effect of radius ratio of the laminated disk on the bending behaviors of the system or stress and displacement fields. Based on the presented diagrams in Fig. 11, when the radius ratio of the laminated disk increases, the displacement fields increase, and stress fields decrease. Also, the radius ratio has the most impressive impact on the stress and displacement fields along the z-direction.

9 Conclusion

In this research, bending analysis of the MHLNCRCP/MHLNCRAP resting on linear and torsional elastic foundations based on three-dimensional poroelasticity theory for various boundary conditions was presented. The SS-DQM was presented to examine the bending behavior of MHLNCRACP/MHLNCRAAP. For prediction of the bulk material properties of the multi-scale composite, Halpin–Tsai equations and fiber micromechanics were presented. The carbon nanotubes were supposed to be randomly oriented and uniformly distributed through the matrix of epoxy resin. Afterward, a parametric study was done to present the effects of stacking sequence, various types of sandwich circular/annular plates, linear and torsional gradient elastic foundation, and Biot's coefficient on the bending characteristics of the composite structure. Finally, the most bolded results of this paper were as follows:

- The bending behavior of the system improves owing to increase the γ factor.
- The bending behavior of the laminated system improves due to increasing the value of Winkler and Pasternak factors, and stress distribution becomes more uniform.

Table 4 Effect of elastic and poroelastic factors on the stress and displacement fields of the laminated structure with $R_o/R_i = 2$, $h = 0.01R_i$, $W_{CNT} = 0.02$, $V_F = 0.8$, [90°/0°/90°/0°/90°], $K_{wo} = K_{po} = 0$, $K_{r10} = K_{r20} = 0$, $\theta_o = \pi/4$, $f_1 = f_2 = P_1 = P_2 = 0.1$, clamped–clamped boundary conditions, and MHLNCAP

	K^p	$\overline{\sigma}_z$	$\overline{u}_r$	$\overline{u}_\theta$	$\overline{u}_z$	$\overline{\tau}_{rz}$	$\overline{\tau}_{\theta z}$	$\overline{\sigma}_r$	$\overline{\sigma}_\theta$	$\overline{\tau}_{r\theta}$
a	$K^p \neq 0$	− 0.3526	− 5.8332	− 2.8774	− 761.82	21.2169	− 0.0936	457.655	15.538	− 0.7765
	$K^p = 0$	− 0.3185	− 6.2127	− 3.1988	− 799.297	19.015	− 0.0834	417.22	13.3429	− 0.8795
b	$K^p \neq 0$	0.0196	− 14.3392	− 4.7053	− 1503.64	17.8866	− 0.1578	160.0671	36.6311	− 1.6921
	$K^p = 0$	0.0224	− 15.3393	− 5.4732	− 1621.78	16.0638	− 0.1429	145.2574	33.0851	− 2.0792
c	$K^p \neq 0$	0.0675	− 23.1319	− 7.4822	− 1960.39	14.9386	− 0.1929	128.7463	56.10861	− 2.6966
	$K^p = 0$	0.0713	− 24.5512	− 8.3752	− 2095.34	13.8053	− 0.1810	115.762	52.9891	− 3.1148

a: [90°/0°/90°]
b: [90°/0°/90°/0°/90°]
c: [90°/0°/90°/0°/90°/0°/90°]

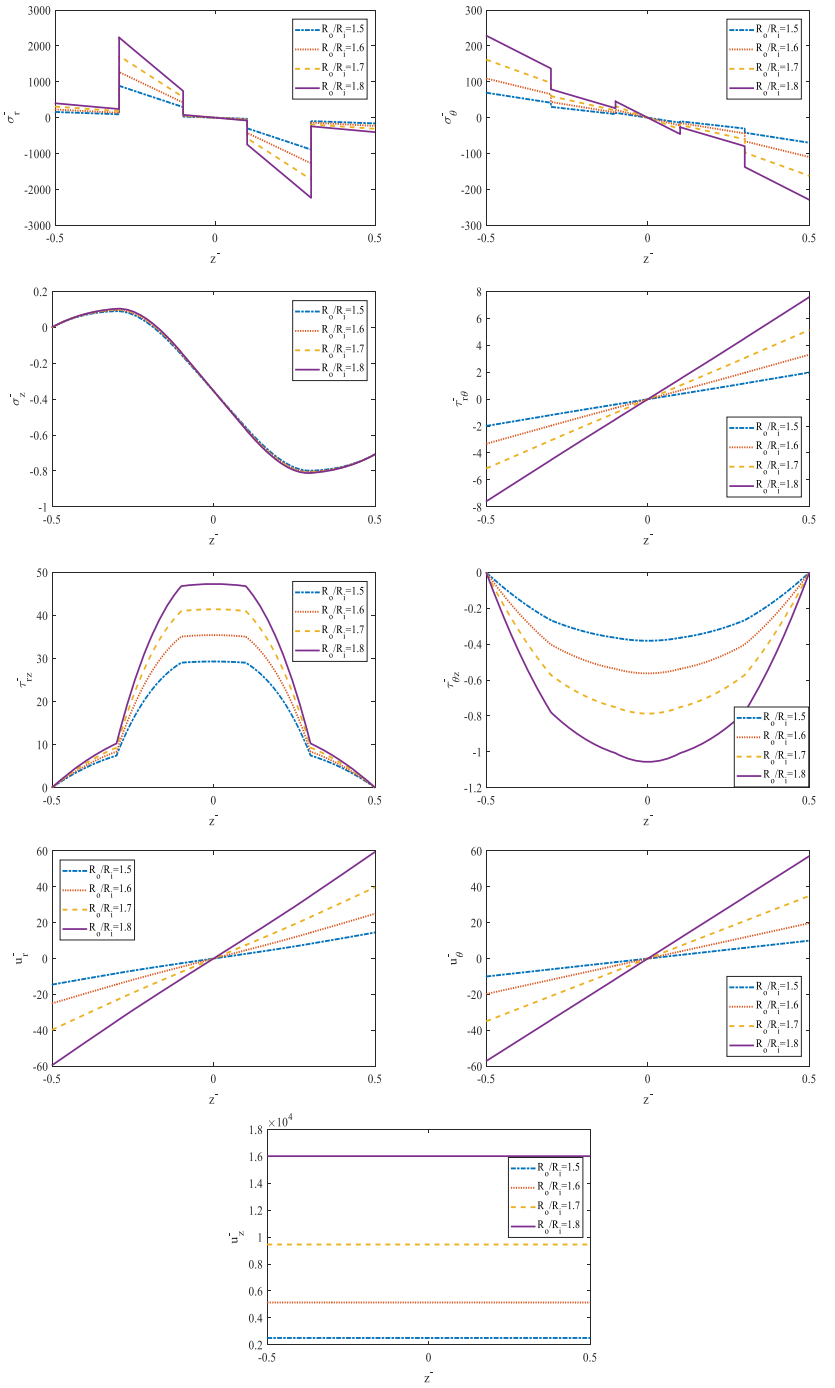

Fig. 11 Effect of R_o/R_i on the stress and displacement fields of the laminated structure with $h = 0.01R_i$, $W_{CNT} = 0.02$, $V_F = 0.8$, [90°/0°/90°/0°/90°], $K_{wo} = K_{po} = 100$, $K_{r10} = K_{r20} = 100$, $\theta_o = \pi/4$, $f_1 = f_2 = P_1 = P_2 = 0.1$, clamped–clamped boundary conditions, and MHLNCAP

- If the laminated structure is under sinusoidal external pressure, we can see that the sensitivity of the static response to the layers' characteristics decreases.
- The impact of external pressure on the hoop shear stress, radial stress, and radial shear stress of the laminated circular plate becomes more considerable in the middle layers.
- K^{p} factor and number of laminated layers have a positive effect on the bending behaviors of the system.

Appendix

$$G=\begin{bmatrix} 0 & 0 & 0 & 0 & a_1 & -\frac{1}{r}\frac{\partial}{\partial\theta} \\ 0 & 0 & 0 & \frac{\partial}{\partial r} & \frac{1}{\overline{Q}_{55}} & 0 \\ 0 & 0 & 0 & -\frac{1}{r}\frac{\partial}{\partial\theta} & 0 & \frac{1}{\overline{Q}_{44}} \\ a_2 & a_3 & a_4 & 0 & 0 & 0 \\ a_5 & a_6 & a_7 & 0 & 0 & 0 \\ -\frac{\overline{Q}^*_{23}}{r\overline{Q}^*_{33}}\frac{\partial}{\partial\theta} & a_8 & a_9 & 0 & 0 & 0 \end{bmatrix}$$

$$a_1=-\frac{\partial}{\partial r}-\frac{1}{r},\quad a_2=\frac{1}{\bar{Q}^*_{33}},\quad a_3=-\frac{\bar{Q}^*_{13}}{\bar{Q}^*_{33}}\frac{\partial}{\partial r}-\frac{\bar{Q}^*_{23}}{r\bar{Q}^*_{33}},\quad a_4=-\frac{\bar{Q}^*_{13}}{r\bar{Q}^*_{33}}\frac{\partial}{\partial\theta}$$

$$a_5=-\frac{\bar{Q}^*_{13}}{\bar{Q}^*_{33}}\frac{\partial}{\partial r}-\left(\frac{\bar{Q}^*_{13}-\bar{Q}^*_{23}}{\bar{Q}^*_{33}}\right)$$

$$a_6=-\left(\overline{Q}^*_{11}-\frac{\overline{Q}^{*2}_{13}}{\overline{Q}^*_{33}}\right)\frac{\partial^2u_r}{\partial r^2}-\frac{1}{r}\left(\overline{Q}^*_{11}-\frac{\overline{Q}^{*2}_{13}}{\overline{Q}^*_{33}}\right)\frac{\partial u_r}{\partial r}$$
$$-\frac{1}{r^2}\left(\frac{\overline{Q}^*_{12}\overline{Q}^*_{33}+\overline{Q}^{*2}_{23}-\overline{Q}^*_{13}\overline{Q}^*_{23}-\overline{Q}^*_{22}\overline{Q}^*_{33}}{\overline{Q}^*_{33}}\right)$$

$$a_7=-\frac{1}{r}\left(\bar{Q}^*_{12}+\bar{Q}_{66}-\frac{\bar{Q}^*_{13}\bar{Q}^*_{23}}{\bar{Q}^*_{33}}\right)\frac{\partial^2u_\theta}{\partial r\partial\theta}$$
$$-\frac{1}{r^2}\left(\frac{\bar{Q}^*_{12}\bar{Q}^*_{33}+\bar{Q}^{*2}_{23}-\bar{Q}^*_{13}\bar{Q}^*_{23}-\bar{Q}^*_{22}\bar{Q}^*_{33}}{\bar{Q}^*_{33}}\right)\frac{\partial u_\theta}{\partial\theta}$$
$$-\frac{\bar{Q}_{66}}{r^2}\frac{\partial^2u_r}{\partial\theta^2}-\frac{1}{r^2}\left(\frac{\bar{Q}^*_{12}\bar{Q}^*_{33}+\bar{Q}^{*2}_{23}-\bar{Q}^*_{13}\bar{Q}^*_{23}-\bar{Q}^*_{22}\bar{Q}^*_{33}}{\bar{Q}^*_{33}}\right)u_r$$

$$a_8=-\frac{1}{r}\left(\overline{Q}^*_{12}+\overline{Q}_{66}-\frac{\overline{Q}^*_{13}\overline{Q}^*_{23}}{\overline{Q}^*_{33}}\right)\frac{\partial^2u_r}{\partial\theta\partial r}-\frac{1}{r^2}\left(\overline{Q}^*_{22}+2\overline{Q}_{66}-\frac{\overline{Q}^{*2}_{23}}{\overline{Q}^*_{33}}\right)\frac{\partial u_r}{\partial\theta}$$

$$a_9=-\overline{Q}_{66}\frac{\partial^2u_\theta}{\partial^2r}-\frac{\overline{Q}_{66}}{r}\frac{\partial u_\theta}{\partial r}-\frac{1}{r^2}\left(\overline{Q}^*_{22}-\frac{\overline{Q}^{*2}_{23}}{\overline{Q}^*_{33}}\right)\frac{\partial^2u_\theta}{\partial^2\theta}+\frac{2\overline{Q}^*_{66}}{r^2}u_\theta$$

Annular plate

Simply–simply

$$\overline{G}_{\mathrm{SS}}=\begin{bmatrix} (0)_{(N-2)(N-2)} & (0)_{(N-2)(N)} & (0)_{(N-2)(N-2)} & (0)_{(N-2)(N-2)} & a_1 & \frac{h}{R_m}\frac{m}{\overline{r}_{i1}}I_{(N-2)(N-2)} \\ (0)_{(N)(N-2)} & (0)_{(N)(N)} & (0)_{(N)(N-2)} & \frac{h}{R_m}\overline{g}_{ijss2} & \frac{I_{(N)(N)}}{\hat{\overline{Q}}_{55}} & (0)_{(N)(N-2)} \\ (0)_{(N-2)(N-2)} & (0)_{(N-2)(N)} & (0)_{(N-2)(N-2)} & -\frac{h}{R_m}\frac{m}{\overline{r}_{i1}}I_{(N-2)(N-2)} & (0)_{(N-2)(N)} & \frac{I_{(N-2)(N-2)}}{\hat{\overline{Q}}_{44}} \\ a_2 & a_3 & a_4 & (0)_{(N-2)(N-2)} & (0)_{(N-2)(N)} & (0)_{(N-2)(N-2)} \\ a_5 & a_6+f_{ss} & a_7 & (0)_{(N)(N-2)} & (0)_{(N)(N)} & (0)_{(N)(N-2)} \\ -\frac{h}{R_m}\frac{\hat{\overline{Q}}_{23}}{\hat{\overline{Q}}_{33}}\frac{m}{\overline{r}_{i1}}I_{(N-2)(N-2)} & a_8 & a_9 & (0)_{(N-2)(N-2)} & (0)_{(N-2)(N)} & (0)_{(N-2)(N-2)} \end{bmatrix}$$

$$a_1=-\frac{h}{R_m}\overline{g}_{ijss1}-\frac{h}{R_m}\frac{I_{(N-2)(N)}}{\overline{r}_{i2}},\quad a_2=\frac{h}{R_m}\frac{I_{(N-2)(N-2)}}{\hat{\overline{Q}}_{33}},$$

$$a_3=-\left(\frac{h}{R_m}\right)^2\frac{\hat{\overline{Q}}_{13}}{\hat{\overline{Q}}_{33}}\overline{g}_{ijss1}-\left(\frac{h}{R_m}\right)^2\frac{\hat{\overline{Q}}_{23}}{\overline{r}_{i2}\hat{\overline{Q}}_{33}}I_{(N-2)(N)}$$

$$a_4=\left(\frac{h}{R_m}\right)^2\frac{\hat{\overline{Q}}_{13}}{\hat{\overline{Q}}_{33}}\frac{m}{\overline{r}_{i1}}I_{(N-2)(N-2)},$$

$$a_5=\left(\frac{h}{R_m}\right)-\frac{\hat{\overline{Q}}_{13}}{\hat{\overline{Q}}_{33}}\overline{g}_{ijss2}-\left(\frac{h}{R_m}\right)\left(\frac{\hat{\overline{Q}}_{13}-\hat{\overline{Q}}_{23}}{\hat{\overline{Q}}_{33}}\right)I_{(N)(N-2)}$$

$$a_6=-\left(\frac{h}{R_m}\right)^2\left(\hat{\overline{Q}}_{11}-\frac{\hat{\overline{Q}}_{13}^2}{\hat{\overline{Q}}_{33}}\right)\overline{g}^{(2)}_{\mathrm{ijss1}}-\left(\frac{h}{R_m}\right)^2\frac{1}{\overline{r}_{i3}}\left(\hat{\overline{Q}}_{11}-\frac{\hat{\overline{Q}}_{13}^2}{\hat{\overline{Q}}_{33}}\right)\overline{g}_{\mathrm{ijss3}}$$
$$-\left(\frac{h}{R_m}\right)^2\frac{1}{\overline{r}_{i2}^2}\left(\frac{\hat{\overline{Q}}_{12}\hat{\overline{Q}}_{33}+\hat{\overline{Q}}_{23}^2-\hat{\overline{Q}}_{13}\hat{\overline{Q}}_{23}-\hat{\overline{Q}}_{22}\hat{\overline{Q}}_{33}}{\hat{\overline{Q}}_{33}}\right)I_{(N)(N)}$$

$$a_7=\left(\frac{h}{R_m}\right)^2\frac{m}{\overline{r}_{i4}}\left(\hat{\overline{Q}}_{12}+\hat{\overline{Q}}_{66}-\frac{\hat{\overline{Q}}_{13}\hat{\overline{Q}}_{23}}{\hat{\overline{Q}}_{33}}\right)\overline{g}_{ijss2}$$
$$+\left(\frac{h}{R_m}\right)^2\frac{m}{\overline{r}_{i3}^2}\left(\frac{\hat{\overline{Q}}_{12}\hat{\overline{Q}}_{33}+\hat{\overline{Q}}_{23}^2-\hat{\overline{Q}}_{13}\hat{\overline{Q}}_{23}-\hat{\overline{Q}}_{22}\hat{\overline{Q}}_{33}}{\hat{\overline{Q}}_{33}}\right)I_{(N)(N-2)}$$
$$+\left(\frac{h}{R_m}\right)^2\frac{\hat{\overline{Q}}_{66}}{\overline{r}_{i3}^2}m^2I_{(N)(N-2)}$$
$$-\left(\frac{h}{R_m}\right)^2\frac{1}{\overline{r}_{i3}^2}\left(\frac{\hat{\overline{Q}}_{12}\hat{\overline{Q}}_{33}+\hat{\overline{Q}}_{23}^2-\hat{\overline{Q}}_{13}\hat{\overline{Q}}_{23}-\hat{\overline{Q}}_{22}\hat{\overline{Q}}_{33}}{\hat{\overline{Q}}_{33}}\right)I_{(N)(N-2)}$$

$$a_8=-\left(\frac{h}{R_m}\right)^2\frac{m}{\overline{r}_{i2}}\left(\hat{\overline{Q}}_{12}+\hat{\overline{Q}}_{66}-\frac{\hat{\overline{Q}}_{13}\hat{\overline{Q}}_{23}}{\hat{\overline{Q}}_{33}}\right)\overline{g}_{\mathrm{ijss1}}$$
$$-\left(\frac{h}{R_m}\right)^2\frac{m}{\overline{r}_{i4}^2}\left(\hat{\overline{Q}}_{22}+2\hat{\overline{Q}}_{66}-\frac{\hat{\overline{Q}}_{23}^2}{\hat{\overline{Q}}_{33}}\right)I_{(N-2)(N)}$$

$$a_9=-\left(\frac{h}{R_m}\right)^2\hat{\overline{Q}}_{66}\overline{g}^{(2)}_{ijss2}-\left(\frac{h}{R_m}\right)^2\frac{\hat{\overline{Q}}_{66}}{\overline{r}_{i1}}\overline{g}_{ijss4}$$

$$+\left(\frac{h}{R_m}\right)^2\frac{m^2}{\bar{r}_{i1}^2}\left(\hat{\bar{Q}}_{22}-\frac{\hat{\bar{Q}}_{23}^2}{\hat{\bar{Q}}_{33}}\right)I_{(N-2)(N-2)}+\left(\frac{h}{R_m}\right)^2\frac{2\hat{\bar{Q}}_{66}}{\bar{r}_{i1}^2}I_{(N-2)(N-2)}$$

$$\bar{g}_{ijss1}=\bar{g}_{ij}(i=2,...,N-1,\ j=1,...,N),$$
$$\bar{g}_{ijss2}=\bar{g}_{ij}(i=1,...,N,\ j=2,...,N-1)$$
$$g_{ijss3}=g_{ij}(i=1,...,N;\ j=1,...,N),$$
$$\bar{g}^{(2)}_{ijss1}=\bar{g}_{ij}\times\bar{g}_{ij}(i=1,...,N;\ j=1,...,N)$$
$$\bar{g}^{(2)}_{ijss2}=\bar{g}_{ij}\times\bar{g}_{ij}(i=2,...,N-1;\ j=2,...,N-1)$$

$$f_{ss}=\left(\frac{h}{R_m}\right)^2\left(\frac{\hat{\bar{Q}}_{11}\hat{\bar{Q}}_{33}-\hat{\bar{Q}}_{13}^2}{\hat{\bar{Q}}_{33}}\right)\left(\bar{g}_{i1}\bar{g}_{1j}+\bar{g}_{iN}\bar{g}_{Nj}\right)$$
$$+\left(\frac{h}{R_m}\right)^2\frac{1}{\bar{r}_{i3}}\left(\frac{\hat{\bar{Q}}_{12}\hat{\bar{Q}}_{33}-\hat{\bar{Q}}_{13}\hat{\bar{Q}}_{23}}{\hat{\bar{Q}}_{33}}\right)$$
$$(\bar{g}_{i1}+\bar{g}_{iN});\ (i=1,...,N;\ j=1,...,N)$$

$$\left(\frac{1}{\bar{r}_{i1}}\right)_{SS}=\begin{cases}\frac{1}{\bar{r}} & i=j\\ 0 & i\neq j\end{cases}\quad(i,j=2,...,N-1),\quad\left(\frac{1}{\bar{r}_{i2}}\right)_{SS}$$
$$=\begin{cases}\frac{1}{\bar{r}} & i=j\\ 0 & i\neq j\end{cases}\quad(i=2,...,N-1;j=1,...,N)$$

$$\left(\frac{1}{\bar{r}_{i3}}\right)_{SS}=\begin{cases}\frac{1}{\bar{r}} & i=j\\ 0 & i\neq j\end{cases}\quad(i,j=1,...,N),\quad\left(\frac{1}{\bar{r}_{i4}}\right)_{SS}$$
$$=\begin{cases}\frac{1}{\bar{r}} & i=j\\ 0 & i\neq j\end{cases}\quad(i=1,...,N;j=2,...,N-1)$$

$$\left(\frac{1}{\bar{r}_{i1}}\right)^2_{SS}=\begin{cases}\left(\frac{1}{\bar{r}}\right)^2 & i=j\\ 0 & i\neq j\end{cases}\quad(i,j=2,...,N-1),\quad\left(\frac{1}{\bar{r}_{i2}}\right)^2_{SS}$$
$$=\begin{cases}\left(\frac{1}{\bar{r}}\right)^2 & i=j\\ 0 & i\neq j\end{cases}\quad(i,j=1,...,N),$$
$$\left(\frac{1}{\bar{r}_{i3}}\right)^2_{SS}=\begin{cases}\left(\frac{1}{\bar{r}}\right)^2 & i=j\\ 0 & i\neq j\end{cases}\quad(i=1,...,N;j=2,...,N-1)$$
$$\left(\frac{1}{\bar{r}_{i4}}\right)^2_{SS}=\begin{cases}\left(\frac{1}{\bar{r}}\right)^2 & i=j\\ 0 & i\neq j\end{cases}\quad(i=2,...,N-1;j=1,...,N)$$

Clamped–Clamped

$$\overline{G}_{CC}=\begin{bmatrix}(0)_{(N-2)(N-2)} & (0)_{(N-2)(N-2)} & (0)_{(N-2)(N-2)} & f_{cc1} & a_1 & \frac{h}{R_m}\frac{m}{\bar{r}_{i1}}I_{(N-2)(N-2)}\\ (0)_{(N-2)(N-2)} & (0)_{(N-2)(N-2)} & (0)_{(N-2)(N-2)} & g_{ijcc} & \frac{I_{(N-2)(N-2)}}{\hat{\bar{Q}}_{55}} & (0)_{(N-2)(N-2)}\\ (0)_{(N-2)(N-2)} & (0)_{(N-2)(N-2)} & (0)_{(N-2)(N-2)} & -\frac{h}{R_m}\frac{m}{\bar{r}_{i1}}I_{(N-2)(N-2)} & (0)_{(N-2)(N-2)} & \frac{I_{(N-2)(N-2)}}{\hat{\bar{Q}}_{44}}\\ a_2 & a_3 & a_4 & (0)_{(N-2)(N-2)} & (0)_{(N-2)(N-2)} & (0)_{(N-2)(N-2)}\\ a_5 & a_6+f_{cc2} & a_7 & (0)_{(N-2)(N-2)} & (0)_{(N-2)(N-2)} & (0)_{(N-2)(N-2)}\\ -\frac{h}{R_m}\frac{\hat{\bar{Q}}_{23}}{\hat{\bar{Q}}_{23}}\frac{m}{\bar{r}_{i1}}I_{(N-2)(N-2)} & a_8 & a_9 & (0)_{(N-2)(N-2)} & (0)_{(N-2)(N-2)} & (0)_{(N-2)(N-2)}\end{bmatrix}$$

$$a_1 = -\frac{h}{R_m}\bar{g}_{ijcc} - \frac{h}{R_m}\frac{I_{(N-2)(N-2)}}{\bar{r}_{i1}},\quad a_2 = \frac{h}{R_m}\frac{I_{(N-2)(N-2)}}{\hat{\bar{Q}}_{33}},$$

$$a_3 = -\left(\frac{h}{R_m}\right)^2\frac{\hat{\bar{Q}}_{13}}{\hat{\bar{Q}}_{33}}\bar{g}_{ijcc} - \left(\frac{h}{R_m}\right)^2\frac{\hat{\bar{Q}}_{23}}{\bar{r}_{i1}\hat{\bar{Q}}_{33}}I_{(N-2)(N-2)}$$

$$a_4 = \left(\frac{h}{R_m}\right)^2\frac{\hat{\bar{Q}}_{13}}{\hat{\bar{Q}}_{33}}\frac{m}{\bar{r}_{i1}}I_{(N-2)(N-2)},$$

$$a_5 = -\frac{h}{R_m}\frac{\hat{\bar{Q}}_{13}}{\hat{\bar{Q}}_{33}}\bar{g}_{ijcc} - \frac{h}{R_m}\left(\frac{\hat{\bar{Q}}_{13} - \hat{\bar{Q}}_{23}}{\hat{\bar{Q}}_{33}}\right)I_{(N-2)(N-2)}$$

$$a_6 = -\left(\frac{h}{R_m}\right)^2\left(\hat{\bar{Q}}_{11} - \frac{\hat{\bar{Q}}_{13}^2}{\hat{\bar{Q}}_{33}}\right)\bar{g}^{(2)}_{ijcc} - \left(\frac{h}{R_m}\right)^2\frac{1}{\bar{r}_{i1}}\left(\hat{\bar{Q}}_{11} - \frac{\hat{\bar{Q}}_{13}^2}{\hat{\bar{Q}}_{33}}\right)\bar{g}_{ijcc}$$
$$- \left(\frac{h}{R_m}\right)^2\frac{1}{\bar{r}_{i1}^2}\left(\frac{\hat{\bar{Q}}_{12}\hat{\bar{Q}}_{33} + \hat{\bar{Q}}_{23}^2 - \hat{\bar{Q}}_{13}\hat{\bar{Q}}_{23} - \hat{\bar{Q}}_{22}\hat{\bar{Q}}_{33}}{\hat{\bar{Q}}_{33}}\right)I_{(N-2)(N-2)}$$

$$a_7 = \left(\frac{h}{R_m}\right)^2\frac{m}{\bar{r}_{i1}}\left(\hat{\bar{Q}}_{12} + \hat{\bar{Q}}_{66} - \frac{\hat{\bar{Q}}_{13}\hat{\bar{Q}}_{23}}{\hat{\bar{Q}}_{33}}\right)\bar{g}_{ijcc}$$
$$+ \left(\frac{h}{R_m}\right)^2\frac{m}{\bar{r}_{i1}^2}\left(\frac{\hat{\bar{Q}}_{12}\hat{\bar{Q}}_{33} + \hat{\bar{Q}}_{23}^2 - \hat{\bar{Q}}_{13}\hat{\bar{Q}}_{23} - \hat{\bar{Q}}_{22}\hat{\bar{Q}}_{33}}{\hat{\bar{Q}}_{33}}\right)I_{(N-2)(N-2)}$$
$$+ \left(\frac{h}{R_m}\right)^2\frac{\hat{\bar{Q}}_{66}}{\bar{r}_{i1}^2}m^2 I_{(N-2)(N-2)}$$
$$- \left(\frac{h}{R_m}\right)^2\frac{1}{\bar{r}_{i1}^2}\left(\frac{\hat{\bar{Q}}_{12}\hat{\bar{Q}}_{33} + \hat{\bar{Q}}_{23}^2 - \hat{\bar{Q}}_{13}\hat{\bar{Q}}_{23} - \hat{\bar{Q}}_{22}\hat{\bar{Q}}_{33}}{\hat{\bar{Q}}_{33}}\right)I_{(N-2)(N-2)}$$

$$a_8 = -\left(\frac{h}{R_m}\right)^2\frac{m}{\bar{r}_{i1}}\left(\hat{\bar{Q}}_{12} + \hat{\bar{Q}}_{66} - \frac{\hat{\bar{Q}}_{13}\hat{\bar{Q}}_{23}}{\hat{\bar{Q}}_{33}}\right)\bar{g}_{ijcc}$$
$$- \left(\frac{h}{R_m}\right)^2\frac{m}{\bar{r}_{i1}^2}\left(\hat{\bar{Q}}_{22} + 2\hat{\bar{Q}}_{66} - \frac{\hat{\bar{Q}}_{23}^2}{\hat{\bar{Q}}_{33}}\right)I_{(N-2)(N-2)}$$

$$a_9 = -\left(\frac{h}{R_m}\right)^2\hat{\bar{Q}}_{66}\bar{g}^{(2)}_{ijcc} - \left(\frac{h}{R_m}\right)^2\frac{\hat{\bar{Q}}_{66}}{\bar{r}_{i1}}\bar{g}_{ijcc} + \left(\frac{h}{R_m}\right)^2\frac{m^2}{\bar{r}_{i1}^2}\left(\hat{\bar{Q}}_{22} - \frac{\hat{\bar{Q}}_{23}^2}{\hat{\bar{Q}}_{33}}\right)I_{(N-2)(N-2)}$$
$$+ \left(\frac{h}{R_m}\right)^2\frac{2\hat{\bar{Q}}_{66}}{\bar{r}_{i1}^2}I_{(N-2)(N-2)}$$

$$\bar{g}_{ijcc} = \bar{g}_{ij}(i = 2, ..., N-1, j = 2, ..., N-1),$$
$$\bar{g}^{(2)}_{ijcc} = \bar{g}_{ij} \times \bar{g}_{ij}(i = 2, ..., N-1, j = 2, ..., N-1)$$

$$f_{cc1} = -\left(\frac{h}{R_m}\right)^2 \hat{\overline{Q}}_{55}\left(\overline{g}_{i1}\overline{g}_{1j} + \overline{g}_{iN}\overline{g}_{Nj}\right);\ \ (i = 2, ..., N-1; j = 2, ..., N-1)$$

$$f_{cc2} = -\left(\frac{h}{R_m}\right)^2 \frac{\hat{\overline{Q}}_{13}^2}{\hat{\overline{Q}}_{33}}\left(\overline{g}_{i1}\overline{g}_{1j} + \overline{g}_{iN}\overline{g}_{Nj}\right);\ \ (i = 2, ..., N-1; j = 2, ..., N-1)$$

$$\left(\frac{1}{\overline{r}_{i1}}\right)_{CC} = \begin{cases} \frac{1}{\overline{r}} & i = j \\ 0 & i \neq j \end{cases} \quad (i, j = 2, ..., N-1), \quad \left(\frac{1}{\overline{r}_{i1}}\right)^2_{CC} = \begin{cases} \left(\frac{1}{\overline{r}}\right)^2 & i = j \\ 0 & i \neq j \end{cases} \quad (i, j = 2, ..., N-1)$$

Clamped–Simply

$$\overline{G}_{CS} = \begin{bmatrix} (0)_{(N-2)(N-2)} & (0)_{(N-2)(N)} & (0)_{(N-2)(N-2)} & f_{cs1} & a_1 & \frac{h}{R_m}\frac{m}{\overline{r}_{i2}} I_{(N-2)(N)} \\ (0)_{(N-2)(N-2)} & (0)_{(N-2)(N)} & (0)_{(N-2)(N-2)} & \frac{h}{R_m} g_{ijcc} & \frac{I_{(N-2)(N)}}{\hat{\overline{Q}}_{55}} & (0)_{(N-2)(N-2)} \\ (0)_{(N-2)(N-2)} & (0)_{(N-2)(N)} & (0)_{(N-2)(N-2)} & -\frac{m}{\overline{r}_{i1}} I_{(N-2)(N-2)} & (0)_{(N-2)(N)} & \frac{I_{(N-2)(N-2)}}{\hat{\overline{Q}}_{44}} \\ a_2 & a_3 & a_4 & (0)_{(N-2)(N-2)} & (0)_{(N-2)(N)} & (0)_{(N-2)(N-2)} \\ a_5 & a_6 + f_{cs2} + f_{cs3} & a_7 & (0)_{(N-2)(N-2)} & (0)_{(N-2)(N)} & (0)_{(N-2)(N-2)} \\ -\frac{h}{R_m}\frac{\hat{\overline{Q}}_{23}}{\hat{\overline{Q}}_{33}}\frac{m}{\overline{r}_{i1}} I_{(N-2)(N-2)} & a_8 & a_9 & (0)_{(N-2)(N-2)} & (0)_{(N-2)(N)} & (0)_{(N-2)(N-2)} \end{bmatrix}$$

$$a_4 = \left(\frac{h}{R_m}\right)^2 \frac{\hat{\overline{Q}}_{13}}{\hat{\overline{Q}}_{33}}\frac{m}{\overline{r}_{i1}} I_{(N-2)(N-2)},\ \ a_5 = -\frac{h}{R_m}\frac{\hat{\overline{Q}}_{13}}{\hat{\overline{Q}}_{33}}\overline{g}_{ijcs2} - \frac{h}{R_m}\left(\frac{\hat{\overline{Q}}_{13} - \hat{\overline{Q}}_{23}}{\hat{\overline{Q}}_{33}}\right) I_{(N-2)(N-2)}$$

$$a_4 = \left(\frac{h}{R_m}\right)^2 \frac{\hat{\overline{Q}}_{13}}{\hat{\overline{Q}}_{33}}\frac{m}{\overline{r}_{i1}} I_{(N-2)(N-2)},\ \ a_5 = -\frac{h}{R_m}\frac{\hat{\overline{Q}}_{13}}{\hat{\overline{Q}}_{33}}\overline{g}_{ijcs2} - \frac{h}{R_m}\left(\frac{\hat{\overline{Q}}_{13} - \hat{\overline{Q}}_{23}}{\hat{\overline{Q}}_{33}}\right) I_{(N-2)(N-2)}$$

$$a_6 = \left(\frac{h}{R_m}\right)^2 \left(\hat{\overline{Q}}_{11} - \frac{\hat{\overline{Q}}_{13}^2}{\hat{\overline{Q}}_{33}}\right)\overline{g}^{(2)}_{ijcs} - \left(\frac{h}{R_m}\right)^2 \frac{1}{\overline{r}_{i2}}\left(\hat{\overline{Q}}_{11} - \frac{\hat{\overline{Q}}_{13}^2}{\hat{\overline{Q}}_{33}}\right)\overline{g}_{ijcs1} - \left(\frac{h}{R_m}\right)^2 \frac{1}{\overline{r}_{i2}^2}\left(\frac{\hat{\overline{Q}}_{12}\hat{\overline{Q}}_{33} + \hat{\overline{Q}}_{23}^2 - \hat{\overline{Q}}_{13}\hat{\overline{Q}}_{23} - \hat{\overline{Q}}_{22}\hat{\overline{Q}}_{33}}{\hat{\overline{Q}}_{33}}\right) I_{(N-2)(N)}$$

$$a_7 = \left(\frac{h}{R_m}\right)^2 \frac{m}{\overline{r}_{i1}}\left(\hat{\overline{Q}}_{12} + \hat{\overline{Q}}_{66} - \frac{\hat{\overline{Q}}_{13}\hat{\overline{Q}}_{23}}{\hat{\overline{Q}}_{33}}\right)\overline{g}_{ijcs2} + \left(\frac{h}{R_m}\right)^2 \frac{m}{\overline{r}_{i1}^2}\left(\frac{\hat{\overline{Q}}_{12}\hat{\overline{Q}}_{33} + \hat{\overline{Q}}_{23}^2 - \hat{\overline{Q}}_{13}\hat{\overline{Q}}_{23} - \hat{\overline{Q}}_{22}\hat{\overline{Q}}_{33}}{\hat{\overline{Q}}_{33}}\right) I_{(N-2)(N-2)} + \left(\frac{h}{R_m}\right)^2 \frac{\hat{\overline{Q}}_{66}}{\overline{r}_{i1}^2} m^2 I_{(N-2)(N-2)} - \left(\frac{h}{R_m}\right)^2 \frac{1}{\overline{r}_{i1}^2}\left(\frac{\hat{\overline{Q}}_{12}\hat{\overline{Q}}_{33} + \hat{\overline{Q}}_{23}^2 - \hat{\overline{Q}}_{13}\hat{\overline{Q}}_{23} - \hat{\overline{Q}}_{22}\hat{\overline{Q}}_{33}}{\hat{\overline{Q}}_{33}}\right) I_{(N-2)(N-2)}$$

$$a_8 = -\left(\frac{h}{R_m}\right)^2 \frac{m}{\overline{r}_{i2}} \left(\hat{\overline{Q}}_{12} + \hat{\overline{Q}}_{66} - \frac{\hat{\overline{Q}}_{13}\hat{\overline{Q}}_{23}}{\hat{\overline{Q}}_{33}}\right) \overline{g}_{\text{ijcs1}} - \left(\frac{h}{R_m}\right)^2 \frac{m}{\overline{r}_{i2}^2} \left(\hat{\overline{Q}}_{22} + 2\hat{\overline{Q}}_{66} - \frac{\hat{\overline{Q}}_{23}^2}{\hat{\overline{Q}}_{33}}\right) I_{(N-2)(N)}$$

$$a_9 = -\left(\frac{h}{R_m}\right)^2 \hat{\overline{Q}}_{66}\overline{g}^{(2)}_{\text{ijcs1}} - \left(\frac{h}{R_m}\right)^2 \frac{\hat{\overline{Q}}_{66}}{\overline{r}_{i1}} \overline{g}_{\text{ijcs1}} + \left(\frac{h}{R_m}\right)^2 \frac{m^2}{\overline{r}_{i1}^2} \left(\hat{\overline{Q}}_{22} - \frac{\hat{\overline{Q}}_{23}^2}{\hat{\overline{Q}}_{33}}\right) I_{(N-2)(N-2)} + \left(\frac{h}{R_m}\right)^2 \frac{2\hat{\overline{Q}}_{66}}{\overline{r}_{i1}^2} I_{(N-2)(N-2)}$$

$$\bar{g}_{\text{ijcs1}} = \bar{g}_{ij}(i = 2, ..., N-1, j = 1, ..., N),$$

$$\bar{g}_{\text{ijcs2}} = \bar{g}_{ij}(i = 2, ..., N-1, j = 2, ..., N-1), \frac{1}{2}$$

$$\bar{g}^{(2)}_{ijcs} = \bar{g}_{ij} \times \bar{g}_{ij}(i = 2, ..., N-1; j = 2, ..., N-1)$$

$$f_{cs1} = -\left(\frac{h}{R_m}\right)^2 \hat{\overline{Q}}_{55}\left(\overline{g}_{i1}\overline{g}_{1j}\right); \quad (i = 2, ..., N-1; j = 2, ..., N-1),$$

$$f_{cs2} = -\left(\frac{h}{R_m}\right)^2 \frac{\hat{\overline{Q}}_{13}^2}{\hat{\overline{Q}}_{33}}\left(\overline{g}_{i1}\overline{g}_{1j}\right); \quad (i = 2, ..., N-1; j = 1, ..., N)$$

$$f_{cs3} = \left(\frac{h}{R_m}\right)^2 \left(\frac{\hat{\bar{Q}}_{11}\hat{\bar{Q}}_{33} - \hat{\bar{Q}}_{13}^2}{\hat{\bar{Q}}_{33}}\right)\left(\bar{g}_{iN}\bar{g}_{Nj}\right) + \left(\frac{h}{R_m}\right)^2 \frac{1}{\bar{r}_{i2}} \left(\frac{\hat{\bar{Q}}_{12}\hat{\bar{Q}}_{33} - \hat{\bar{Q}}_{13}\hat{\bar{Q}}_{23}}{\hat{\bar{Q}}_{33}}\right)(\bar{g}_{iN}); \quad (i = 2, ..., N-1; j = 1, ..., N)$$

$$\left(\frac{1}{\overline{r}_{i1}}\right)_{CS} = \begin{cases} \frac{1}{\overline{r}} & i = j \\ 0 & i \neq j \end{cases} \quad (i, j = 2, ..., N-1), \quad \left(\frac{1}{\overline{r}_{i2}}\right)_{CS} = \begin{cases} \frac{1}{\overline{r}} & i = j \\ 0 & i \neq j \end{cases} \quad (i = 2, ..., N-1; j = 1, ..., N)$$

$$\left(\frac{1}{\overline{r}_{i1}}\right)^2_{CS} = \begin{cases} \left(\frac{1}{\overline{r}}\right)^2 & i = j \\ 0 & i \neq j \end{cases} \quad (i, j = 2, ..., N-1), \quad \left(\frac{1}{\overline{r}_{i2}}\right)^2_{CS} = \begin{cases} \left(\frac{1}{\overline{r}}\right)^2 & i = j \\ 0 & i \neq j \end{cases} \quad (i = 2, ..., N-1; j = 1, ..., N)$$

Circular plate

Hinged–simply

$$\overline{G}_{HS}=\begin{bmatrix} {}^{(0)}_{(N)(N-2)} & {}^{(0)}_{(N)(N)} & {}^{(0)}_{(N)(N-2)} & f_{hs1} & a_1 & \frac{h}{R_m}\frac{m}{\bar{r}_{i4}}I_{(N)(N-2)} \\ {}^{(0)}_{(N-2)(N-2)} & {}^{(0)}_{(N-2)(N)} & {}^{(0)}_{(N-2)(N-2)} & \frac{h}{R_m}\bar{g}_{ijhs2} & \frac{I_{(N-2)(N)}}{\hat{\bar{Q}}_{55}} & {}^{(0)}_{(N-2)(N-2)} \\ {}^{(0)}_{(N)(N-2)} & {}^{(0)}_{(N)(N)} & {}^{(0)}_{(N)(N-2)} & -\frac{h}{R_m}\frac{m}{\bar{r}_{i4}}I_{(N)(N-2)} & {}^{(0)}_{(N)(N)} & \frac{I_{(N)(N-2)}}{\hat{\bar{Q}}_{44}} \\ a_2 & a_3 & a_4 & {}^{(0)}_{(N)(N-2)} & {}^{(0)}_{(N)(N)} & {}^{(0)}_{(N)(N-2)} \\ a_5 & a_6+f_{hs2} & a_7 & {}^{(0)}_{(N-2)(N-2)} & {}^{(0)}_{(N-2)(N)} & {}^{(0)}_{(N-2)(N-2)} \\ -\frac{h}{R_m}\frac{\hat{\bar{Q}}_{23}}{\hat{\bar{Q}}_{33}}\frac{m}{\bar{r}_{i4}}I_{(N)(N-2)} & a_8 & a_9 & {}^{(0)}_{(N)(N-2)} & {}^{(0)}_{(N)(N)} & {}^{(0)}_{(N)(N-2)} \end{bmatrix}$$

$$a_1=-\frac{h}{R_m}\bar{g}_{ijhs1}-\frac{h}{R_m}\frac{I_{(N)(N)}}{\bar{r}_{i3}},\quad a_2=\frac{h}{R_m}\frac{I_{(N)(N-2)}}{\hat{\bar{Q}}_{33}},$$

$$a_3=-\left(\frac{h}{R_m}\right)^2\frac{\hat{\bar{Q}}_{13}}{\hat{\bar{Q}}_{33}}\bar{g}_{ijhs1}-\left(\frac{h}{R_m}\right)^2\frac{\hat{\bar{Q}}_{23}}{\bar{r}_{i3}\hat{\bar{Q}}_{33}}I_{(N)(N)}$$

$$a_4=\left(\frac{h}{R_m}\right)^2\frac{\hat{\bar{Q}}_{13}}{\hat{\bar{Q}}_{33}}\frac{m}{\bar{r}_{i4}}I_{(N)(N-2)},\quad a_5=-\frac{h}{R_m}\frac{\hat{\bar{Q}}_{13}}{\hat{\bar{Q}}_{33}}\bar{g}_{ijhs3}-\frac{h}{R_m}\left(\frac{\hat{\bar{Q}}_{13}-\hat{\bar{Q}}_{23}}{\hat{\bar{Q}}_{33}}\right)I_{(N-2)(N-2)}$$

$$a_6=-\left(\frac{h}{R_m}\right)^2\left(\hat{\bar{Q}}_{11}-\frac{\hat{\bar{Q}}_{13}^2}{\hat{\bar{Q}}_{33}}\right)\bar{g}^{(2)}_{ijhs1}-\left(\frac{h}{R_m}\right)^2\frac{1}{\bar{r}_{i2}}\left(\hat{\bar{Q}}_{11}-\frac{\hat{\bar{Q}}_{13}^2}{\hat{\bar{Q}}_{33}}\right)\bar{g}_{ijhs4}$$
$$+\left(\frac{h}{R_m}\right)^2\frac{1}{\bar{r}_{i4}^2}\left(\frac{\hat{\bar{Q}}_{12}\hat{\bar{Q}}_{33}+\hat{\bar{Q}}_{23}^2-\hat{\bar{Q}}_{13}\hat{\bar{Q}}_{23}-\hat{\bar{Q}}_{22}\hat{\bar{Q}}_{33}}{\hat{\bar{Q}}_{33}}\right)I_{(N-2)(N)}$$

$$a_7=\left(\frac{h}{R_m}\right)^2\frac{m}{\bar{r}_{i1}}\left(\hat{\bar{Q}}_{12}+\hat{\bar{Q}}_{66}-\frac{\hat{\bar{Q}}_{13}\hat{\bar{Q}}_{23}}{\hat{\bar{Q}}_{33}}\right)\bar{g}_{ijhc2}$$
$$+\left(\frac{h}{R_m}\right)^2\frac{m}{\bar{r}_{i1}^2}\left(\frac{\hat{\bar{Q}}_{12}\hat{\bar{Q}}_{33}+\hat{\bar{Q}}_{23}^2-\hat{\bar{Q}}_{13}\hat{\bar{Q}}_{23}-\hat{\bar{Q}}_{22}\hat{\bar{Q}}_{33}}{\hat{\bar{Q}}_{33}}\right)I_{(N-2)(N-2)}$$
$$+\left(\frac{h}{R_m}\right)^2\frac{\hat{\bar{Q}}_{66}}{\bar{r}_{i1}^2}m^2I_{(N-2)(N-2)}$$
$$-\left(\frac{h}{R_m}\right)^2\frac{1}{\bar{r}_{i1}^2}\left(\frac{\hat{\bar{Q}}_{12}\hat{\bar{Q}}_{33}+\hat{\bar{Q}}_{23}^2-\hat{\bar{Q}}_{13}\hat{\bar{Q}}_{23}-\hat{\bar{Q}}_{22}\hat{\bar{Q}}_{33}}{\hat{\bar{Q}}_{33}}\right)I_{(N-2)(N-2)}$$

$$a_8=-\left(\frac{h}{R_m}\right)^2\frac{m}{\bar{r}_{i3}}\left(\hat{\bar{Q}}_{12}+\hat{\bar{Q}}_{66}-\frac{\hat{\bar{Q}}_{13}\hat{\bar{Q}}_{23}}{\hat{\bar{Q}}_{33}}\right)\bar{g}_{ijhs1}$$
$$-\left(\frac{h}{R_m}\right)^2\frac{m}{\bar{r}_{i2}^2}\left(\hat{\bar{Q}}_{22}+2\hat{\bar{Q}}_{66}-\frac{\hat{\bar{Q}}_{23}^2}{\hat{\bar{Q}}_{33}}\right)I_{(N)(N)}$$

$$a_9=-\left(\frac{h}{R_m}\right)^2\hat{\bar{Q}}_{66}\bar{g}^{(2)}_{ijhs2}-\left(\frac{h}{R_m}\right)^2\frac{\bar{Q}_{66}}{\bar{r}_{i4}}\bar{g}_{ijhs2}$$
$$+\left(\frac{h}{R_m}\right)^2\frac{m^2}{\bar{r}_{i3}^2}\left(\hat{\bar{Q}}_{22}-\frac{\hat{\bar{Q}}_{23}^2}{\hat{\bar{Q}}_{33}}\right)I_{(N)(N-2)}+\left(\frac{h}{R_m}\right)^2\frac{2\hat{\bar{Q}}_{66}}{\bar{r}_{i3}^2}I_{(N)(N-2)}$$

$$\overline{g}_{ijhs1} = \overline{g}_{ij}(i = 1, ..., N, j = 1, ..., N), \quad \overline{g}_{ijhs2} = \overline{g}_{ij}(i = 1, ..., N, j = 2, ..., N-1)$$

$$\overline{g}_{ijhs3} = \overline{g}_{ij}(i = 2, ..., N-1, j = 2, ..., N-1), \quad \overline{g}_{ijhs4} = \overline{g}_{ij}(i = 2, ..., N-1, j = 1, ..., N)$$

$$\bar{g}^{(2)}_{ijhs1} = \bar{g}_{ij} \times \bar{g}_{ij}(i = 2, ..., N-1; j = 1, ..., N),$$
$$\bar{g}^{(2)}_{ijhs2} = \bar{g}_{ij} \times \bar{g}_{ij}(i = 2, ..., N-1; j = 1, ..., N)$$
$$f_{hs1} = -\left(\frac{h}{R_m}\right)^2 \hat{\overline{Q}}_{55}\left(\overline{g}_{i1}\overline{g}_{1j}\right);\ (i = 1, ..., N; j = 1, ..., N)$$

$$f_{hs2} = \left(\frac{h}{R_m}\right)^2 \left(\frac{\hat{\overline{Q}}_{11}\hat{\overline{Q}}_{33} - \hat{\overline{Q}}_{13}^2}{\hat{\overline{Q}}_{33}}\right)\left(\overline{g}_{iN}\overline{g}_{Nj}\right)$$
$$+\left(\frac{h}{R_m}\right)^2 \frac{1}{\overline{r}_{i2}}\left(\frac{\hat{\overline{Q}}_{12}\hat{\overline{Q}}_{33} - \hat{\overline{Q}}_{13}\hat{\overline{Q}}_{23}}{\hat{\overline{Q}}_{33}}\right)\left(\overline{g}_{iN}\right);\ (i = 2, ..., N-1; j = 1, ..., N)$$

$$\left(\frac{1}{\overline{r}_{i1}}\right)_{\mathrm{HS}} = \begin{cases} \frac{1}{\overline{r}} & i = j \\ 0 & i \neq j \end{cases} \quad (i, j = 2, ..., N-1), \quad \left(\frac{1}{\overline{r}_{i2}}\right)_{\mathrm{HS}}$$
$$= \begin{cases} \frac{1}{\overline{r}} & i = j \\ 0 & i \neq j \end{cases} \quad (i = 2, ..., N-1; j = 1, ..., N)$$

$$\left(\frac{1}{\overline{r}_{i3}}\right)_{\mathrm{HS}} = \begin{cases} \frac{1}{\overline{r}} & i = j \\ 0 & i \neq j \end{cases} \quad (i, j = 1, ..., N), \quad \left(\frac{1}{\overline{r}_{i4}}\right)_{\mathrm{HS}}$$
$$= \begin{cases} \frac{1}{\overline{r}} & i = j \\ 0 & i \neq j \end{cases} \quad (i = 1, ..., N; j = 2, ..., N-1)$$

$$\left(\frac{1}{\overline{r}_{i1}}\right)^2_{\mathrm{HS}} = \begin{cases} \left(\frac{1}{\overline{r}}\right)^2 & i = j \\ 0 & i \neq j \end{cases} \quad (i, j = 2, ..., N-1), \quad \left(\frac{1}{\overline{r}_{i2}}\right)^2_{\mathrm{HS}}$$
$$= \begin{cases} \left(\frac{1}{\overline{r}}\right)^2 & i = j \\ 0 & i \neq j \end{cases} \quad (i, j = 1, ..., N),$$
$$\left(\frac{1}{\overline{r}_{i3}}\right)^2_{\mathrm{HS}} = \begin{cases} \left(\frac{1}{\overline{r}}\right)^2 & i = j \\ 0 & i \neq j \end{cases} \quad (i = 1, ..., N; j = 2, ..., N-1)$$
$$\left(\frac{1}{\overline{r}_{i4}}\right)^2_{\mathrm{HS}} = \begin{cases} \left(\frac{1}{\overline{r}}\right)^2 & i = j \\ 0 & i \neq j \end{cases} \quad (i = 2, ..., N-1; j = 1, ..., N)$$

Hinged–clamped

$$\overline{G}_{\mathrm{HC}} = \begin{bmatrix} (0)_{(N)(N-2)} & (0)_{(N)(N-2)} & (0)_{(N)(N-2)} & f_{hc1} & a_1 & \frac{h}{R_m}\frac{m}{\overline{r}_{i2}} I_{(N)(N-2)} \\ (0)_{(N-2)(N-2)} & (0)_{(N-2)(N-2)} & (0)_{(N-2)(N-2)} & \frac{h}{R_m} g_{ijhc2} & \frac{I_{(N-2)(N-2)}}{\hat{\overline{Q}}_{55}} & (0)_{(N-2)(N-2)} \\ (0)_{(N)(N-2)} & (0)_{(N)(N-2)} & (0)_{(N)(N-2)} & -\frac{h}{R_m}\frac{m}{\overline{r}_{i2}} I_{(N)(N-2)} & (0)_{(N)(N-2)} & \frac{I_{(N)(N-2)}}{\hat{\overline{Q}}_{44}} \\ a_2 & a_3 & a_4 & (0)_{(N)(N-2)} & (0)_{(N)(N-2)} & (0)_{(N)(N-2)} \\ a_5 & a_6 + f_{hc2} & a_7 & (0)_{(N-2)(N-2)} & (0)_{(N-2)(N-2)} & (0)_{(N-2)(N-2)} \\ -\frac{h}{R_m}\frac{\hat{\overline{Q}}_{23}}{\hat{\overline{Q}}_{33}}\frac{m}{\overline{r}_{i2}} I_{(N)(N-2)} & a_8 & a_9 & (0)_{(N)(N-2)} & (0)_{(N)(N-2)} & (0)_{(N)(N-2)} \end{bmatrix}$$

$$a_1 = -\frac{h}{R_m}\overline{g}_{\text{ijhc}} - \frac{h}{R_m}\frac{I_{(N)(N-2)}}{\overline{r}_{i2}},\quad a_2 = \frac{h}{R_m}\frac{I_{(N)(N-2)}}{\hat{\overline{Q}}_{33}},$$

$$a_3 = -\left(\frac{h}{R_m}\right)^2\frac{\hat{\overline{Q}}_{13}}{\hat{\overline{Q}}_{33}}\overline{g}_{\text{ijhc1}} - \left(\frac{h}{R_m}\right)^2\frac{\hat{\overline{Q}}_{23}}{\overline{r}_{i2}\hat{\overline{Q}}_{33}}I_{(N)(N-2)}$$

$$a_4 = \left(\frac{h}{R_m}\right)^2\frac{\hat{\overline{Q}}_{13}}{\hat{\overline{Q}}_{33}}\frac{m}{\overline{r}_{i4}}I_{(N)(N-2)},\quad a_5 = -\frac{h}{R_m}\frac{\hat{\overline{Q}}_{13}}{\hat{\overline{Q}}_{33}}\overline{g}_{ijhs3} - \frac{h}{R_m}\left(\frac{\hat{\overline{Q}}_{13} - \hat{\overline{Q}}_{23}}{\hat{\overline{Q}}_{33}}\right)I_{(N-2)(N-2)}$$

$$a_6 = -\left(\frac{h}{R_m}\right)^2\left(\hat{\overline{Q}}_{11} - \frac{\hat{\overline{Q}}_{13}^2}{\hat{\overline{Q}}_{33}}\right)\overline{g}_{ijhc1}^2 - \left(\frac{h}{R_m}\right)^2\frac{1}{\overline{r}_{i1}}\left(\hat{\overline{Q}}_{11} - \frac{\hat{\overline{Q}}_{13}^2}{\hat{\overline{Q}}_{33}}\right)\overline{g}_{ijhc2} + \left(\frac{h}{R_m}\right)^2\frac{1}{\overline{r}_{i1}^2}\left(\frac{\hat{\overline{Q}}_{12}\hat{\overline{Q}}_{33} + \hat{\overline{Q}}_{23}^2 - \hat{\overline{Q}}_{13}\hat{\overline{Q}}_{23} - \hat{\overline{Q}}_{22}\hat{\overline{Q}}_{33}}{\hat{\overline{Q}}_{33}}\right)I_{(N-2)(N-2)}$$

$$a_7 = \left(\frac{h}{R_m}\right)^2\frac{m}{\overline{r}_{i1}}\left(\hat{\overline{Q}}_{12} + \hat{\overline{Q}}_{66} - \frac{\hat{\overline{Q}}_{13}\hat{\overline{Q}}_{23}}{\hat{\overline{Q}}_{33}}\right)\overline{g}_{ijhc2} + \left(\frac{h}{R_m}\right)^2\frac{m}{\overline{r}_{i1}^2}\left(\frac{\hat{\overline{Q}}_{12}\hat{\overline{Q}}_{33} + \hat{\overline{Q}}_{23}^2 - \hat{\overline{Q}}_{13}\hat{\overline{Q}}_{23} - \hat{\overline{Q}}_{22}\hat{\overline{Q}}_{33}}{\hat{\overline{Q}}_{33}}\right)I_{(N-2)(N-2)} + \left(\frac{h}{R_m}\right)^2\frac{\hat{\overline{Q}}_{66}}{\overline{r}_{i1}^2}m^2 I_{(N-2)(N-2)} - \left(\frac{h}{R_m}\right)^2\frac{1}{\overline{r}_{i1}^2}\left(\frac{\hat{\overline{Q}}_{12}\hat{\overline{Q}}_{33} + \hat{\overline{Q}}_{23}^2 - \hat{\overline{Q}}_{13}\hat{\overline{Q}}_{23} - \hat{\overline{Q}}_{22}\hat{\overline{Q}}_{33}}{\hat{\overline{Q}}_{33}}\right)I_{(N-2)(N-2)} + \left(\frac{h}{R_m}\right)^2\frac{\hat{\overline{Q}}_{66}}{\overline{r}_{i1}^2}m^2 I_{(N-2)(N-2)} - \left(\frac{h}{R_m}\right)^2\frac{1}{\overline{r}_{i1}^2}\left(\frac{\hat{\overline{Q}}_{12}\hat{\overline{Q}}_{33} + \hat{\overline{Q}}_{23}^2 - \hat{\overline{Q}}_{13}\hat{\overline{Q}}_{23} - \hat{\overline{Q}}_{22}\hat{\overline{Q}}_{33}}{\hat{\overline{Q}}_{33}}\right)I_{(N-2)(N-2)}$$

$$a_8 = -\left(\frac{h}{R_m}\right)^2\frac{m}{\overline{r}_{i2}}\left(\hat{\overline{Q}}_{12} + \hat{\overline{Q}}_{66} - \frac{\hat{\overline{Q}}_{13}\hat{\overline{Q}}_{23}}{\hat{\overline{Q}}_{33}}\right)\overline{g}_{ijhc1} - \left(\frac{h}{R_m}\right)^2\frac{m}{\overline{r}_{i2}^2}\left(\hat{\overline{Q}}_{22} + 2\hat{\overline{Q}}_{66} - \frac{\hat{\overline{Q}}_{23}^2}{\hat{\overline{Q}}_{33}}\right)I_{(N)(N-2)}$$

$$a_9 = -\left(\frac{h}{R_m}\right)^2\hat{\overline{Q}}_{66}g_{ijhc2}^{(2)} - \left(\frac{h}{R_m}\right)^2\frac{\hat{\overline{Q}}_{66}}{\overline{r}_{i2}}\overline{g}_{ijhc1} + \left(\frac{h}{R_m}\right)^2\frac{m^2}{\overline{r}_{i2}^2}\left(\hat{\overline{Q}}_{22} - \frac{\hat{\overline{Q}}_{23}^2}{\hat{\overline{Q}}_{33}}\right)I_{(N)(N-2)} + \left(\frac{h}{R_m}\right)^2\frac{2\hat{\overline{Q}}_{66}}{\overline{r}_{i2}^2}I_{(N)(N-2)}$$

$$\overline{g}_{ijhc1} = \overline{g}_{ij}(i = 1, ..., N, j = 2, ..., N-1), \quad \overline{g}_{ijhc2} = \overline{g}_{ij}(i = 2, ..., N-1, j = 2, ..., N-1),$$

$$\overline{g}^{(2)}_{ijhc1} = \overline{g}_{ij} \times \overline{g}_{ij}(i = 2, ..., N-1; j = 2, ..., N-1), \quad \overline{g}^{(2)}_{ijhc2} = \overline{g}_{ij} \times \overline{g}_{ij}(i = 2, ..., N-1; j = 2, ..., N-1)$$

$$f_{hc1} = -\left(\frac{h}{R_m}\right)^2 \hat{\overline{Q}}_{55}\left(\overline{g}_{i1}\overline{g}_{1j} + \overline{g}_{iN}\overline{g}_{Nj}\right); \ (i = 1, ..., N; j = 2, ..., N-1),$$

$$f_{hc2} = -\left(\frac{h}{R_m}\right)^2 \frac{\hat{\overline{Q}}^2_{13}}{\hat{\overline{Q}}_{33}}\left(\overline{g}_{iN}\overline{g}_{Nj}\right); \ (i = 2, ..., N-1; j = 2, ..., N-1)$$

$$\left(\frac{1}{\overline{r}_{i1}}\right)_{HC} = \begin{cases} \frac{1}{\overline{r}} & i = j \\ 0 & i \neq j \end{cases} (i, j = 2, ..., N-1), \ \left(\frac{1}{\overline{r}_{i2}}\right)_{HC} = \begin{cases} \frac{1}{\overline{r}} & i = j \\ 0 & i \neq j \end{cases} (i = 1, ..., N; j = 2, ..., N-1)$$

$$\left(\frac{1}{\overline{r}_{i1}}\right)^2_{HC} = \begin{cases} \left(\frac{1}{\overline{r}}\right)^2 & i = j \\ 0 & i \neq j \end{cases} (i, j = 2, ..., N-1), \ \left(\frac{1}{\overline{r}_{i2}}\right)^2_{HC} = \begin{cases} \left(\frac{1}{\overline{r}}\right)^2 & i = j \\ 0 & i \neq j \end{cases} (i = 1, ..., N; j = 2, ..., N-1)$$

References

1. S. Chen, M. Hassanzadeh-Aghdam, R. Ansari, An analytical model for elastic modulus calculation of SiC whisker-reinforced hybrid metal matrix nanocomposite containing SiC nanoparticles. J. Alloy. Compd. **767**, 632–641 (2018)
2. K. Zhang, Q. Huo, Y.-Y. Zhou, H.-H. Wang, G.-P. Li, Y.-W. Wang et al., Textiles/metal–organic frameworks composites as flexible air filters for efficient particulate matter removal. ACS Appl. Mater. Interfaces. **11**, 17368–17374 (2019)
3. K. Zhang, Z. Yang, X. Mao, X.-L. Chen, H.-H. Li, Y.-Y. Wang, Multifunctional textiles/metal: organic frameworks composites for efficient ultraviolet radiation blocking and noise reduction. ACS Appl. Mater. Interfaces. **12**, 55316–55323 (2020)
4. Z. Yang, P. Xu, W. Wei, G. Gao, N. Zhou, G. Wu, Influence of the crosswind on the pantograph arcing dynamics. IEEE Trans. Plasma Sci. **48**, 2822–2830 (2020)
5. C. Liu, F. Wang, L. He, X. Deng, J. Liu, Y. Wu, Experimental and numerical investigation on dynamic responses of the umbrella membrane structure excited by heavy rainfall. J. Vib. Control (2020). https://doi.org/10.1177/1077546320932691
6. C. Liu, F. Wang, X. Deng, S. Pang, J. Liu, Y. Wu et al., Hailstone-induced dynamic responses of pretensioned umbrella membrane structure. Adv. Struct. Eng. (2020). https://doi.org/10.1177/13694332209400149
7. H. Zhang, M. Sun, L. Song, J. Guo, L. Zhang, Fate of NaClO and membrane foulants during in-situ cleaning of membrane bioreactors: Combined effect on thermodynamic properties of sludge. Biochem. Eng. J. **147**, 146–152 (2019)
8. D. Yan, Y. Zheng, W. Wang, Q. Chen, Modeling and dynamic analyses of the bulb turbine blade with crack fault. Appl. Math. Model. **89**, 731–751 (2021)
9. D. Yan, W. Wang, Q. Chen, Fractional-order modeling and nonlinear dynamic analyses of the rotor-bearing-seal system. Chaos Solitons Fract. **133**, 109640 (2020)

10. Y. Yang, Y. Li, J. Yao, S. Iglauer, L. Luquot, K. Zhang et al., Dynamic pore-scale dissolution by CO2-saturated brine in carbonates: Impact of homogeneous versus fractured versus vuggy pore structure. Water Resour. Res. (2020). https://doi.org/10.1029/2019WR026112
11. S. Zhang, R.Y. Pak, J. Zhang, Vertical time-harmonic coupling vibration of an impermeable, rigid, circular plate resting on a finite, poroelastic soil layer. Acta Geotech. (2020). https://doi.org/10.1007/s11440-020-01067-8
12. S.K. Chakrapani, D.J. Barnard, V. Dayal, Nonlinear forced vibration of carbon fiber/epoxy prepreg composite beams: theory and experiment. Compos. B Eng. **91**, 513–521 (2016)
13. S. Emam, M. Eltaher, Buckling and postbuckling of composite beams in hygrothermal environments. Compos. Struct. **152**, 665–675 (2016)
14. S. Maghamikia, J. Jam, Buckling analysis of circular and annular composite plates reinforced with carbon nanotubes using FEM. J. Mech. Sci. Technol. **25**, 2805–2810 (2011)
15. V. Tahouneh, M. Yas, Influence of equivalent continuum model based on the Eshelby-Mori-Tanaka scheme on the vibrational response of elastically supported thick continuously graded carbon nanotube-reinforced annular plates. Polym. Compos. **35**, 1644–1661 (2014)
16. V. Tahouneh, J. Eskandari-Jam, A semi-analytical solution for 3-D dynamic analysis of thick continuously graded carbon nanotube-reinforced annular plates resting on a Two-parameter elastic foundation. Mech. Adv. Compos. Struct. **1**, 113–130 (2014)
17. R. Ansari, J. Torabi, M.F. Shojaei, Buckling and vibration analysis of embedded functionally graded carbon nanotube-reinforced composite annular sector plates under thermal loading. Compos. B Eng. **109**, 197–213 (2017)
18. C. Zuo, J. Sun, J. Li, J. Zhang, A. Asundi, Q. Chen, High-resolution transport-of-intensity quantitative phase microscopy with annular illumination. Sci. Rep. **7**, 1–22 (2017)
19. J. Zhang, J. Sun, Q. Chen, C. Zuo, Resolution analysis in a lens-free on-chip digital holographic microscope. IEEE Trans. Comput. Imaging **6**, 697–710 (2020)
20. Y. Hu, Q. Chen, S. Feng, C. Zuo, Microscopic fringe projection profilometry: a review. Opt. Lasers Eng. **135**, 106192 (2020)
21. Y. Zhang, C. Li, H. Ji, X. Yang, M. Yang, D. Jia et al., Analysis of grinding mechanics and improved predictive force model based on material-removal and plastic-stacking mechanisms. Int. J. Mach. Tools Manuf **122**, 81–97 (2017)
22. D. Chen, J. Yang, S. Kitipornchai, Buckling and bending analyses of a novel functionally graded porous plate using Chebyshev-Ritz method. Arch. Civ. Mech. Eng. **19**, 157–170 (2019)
23. Y.Q. Wang, M.W. Teng, Vibration analysis of circular and annular plates made of 3D graphene foams via Chebyshev-Ritz method. Aerospace Sci. Technol. **95**, 105440 (2019)
24. V.G. Belardi, P. Fanelli, F. Vivio, Ritz method analysis of rectilinear orthotropic composite circular plates undergoing in-plane bending and torsional moments. Mech. Adv. Mater. Struct. (2019). https://doi.org/10.1080/15376494.2019.1614701
25. P. Xiang, Q. Xia, L. Jiang, L. Peng, J. Yan, X. Liu, Free vibration analysis of FG-CNTRC conical shell panels using the kernel particle Ritz element-free method. Compos. Struct. **255**, 112987 (2021)
26. X. Liu, X. Zhao, C. Xie, Exact free vibration analysis for membrane assemblies with general classical boundary conditions. J. Sound Vib. **485**, 115484 (2020)
27. V.G. Belardi, P. Fanelli, F. Vivio, On the radial bending of shear-deformable composite circular plates with rectilinear orthotropy. Eur. J. Mech. A/Solids **86**, 104157 (2021)
28. V.G. Belardi, P. Fanelli, F. Vivio, First-order shear deformation analysis of rectilinear orthotropic composite circular plates undergoing transversal loads. Compos. Part B Eng. **174**, 107015 (2019)
29. R. Vescovini, L. Dozio, M. d'Ottavio, O. Polit, On the application of the Ritz method to free vibration and buckling analysis of highly anisotropic plates. Compos. Struct. **192**, 460–474 (2018)
30. Z. Zhang, C. Luo, Z. Zhao, Application of probabilistic method in maximum tsunami height prediction considering stochastic seabed topography. Nat. Hazards **104**, 2511–2530 (2020)
31. Y. Yang, J. Yao, C. Wang, Y. Gao, Q. Zhang, S. An et al., New pore space characterization method of shale matrix formation by considering organic and inorganic pores. J. Nat. Gas Sci. Eng. **27**, 496–503 (2015)
32. J. Zhang, Q. Chen, J. Sun, L. Tian, C. Zuo, On a universal solution to the transport-of-intensity equation. Opt. Lett. **45**, 3649–3652 (2020)
33. X. Yan, X. Huang, Y. Chen, Y. Liu, L. Xia, T. Zhang et al., A theoretical strategy of pure carbon materials for lightweight and excellent absorption performance. Carbon **174**, 662–672 (2021)
34. A.S.R. Olia, D. Perić, Thermomechanical soil-structure interaction in single energy piles exhibiting reversible interface behavior. Int. J. Geomech. **21**, 04021065 (2021)
35. A. Alibeigloo, Three-dimensional thermoelasticity analysis of graphene platelets reinforced cylindrical panel. Eur. J. Mech. A/Solids **81**, 103941 (2020)

36. M. Shaban, A. Alibeigloo, Global bending analysis of corrugated sandwich panels with integrated piezoelectric layers. J. Sandwich Struct. Mater. **22**, 1055–1073 (2020)
37. A. Rahimi, A. Alibeigloo, M. Safarpour, Three-dimensional static and free vibration analysis of graphene platelet–reinforced porous composite cylindrical shell. J. Vib. Control (2020). https://doi.org/10.1177/1077546320902340
38. M. Safarpour, A. Rahimi, A. Alibeigloo, H. Bisheh, A. Forooghi, Parametric study of three-dimensional bending and frequency of FG-GPLRC porous circular and annular plates on different boundary conditions. Mech. Based Des. Struct. Mach. (2019). https://doi.org/10.1080/15397734.2019.1701491
39. M. Safarpour, A. Rahimi, A. Alibeigloo, Static and free vibration analysis of graphene platelets reinforced composite truncated conical shell, cylindrical shell, and annular plate using theory of elasticity and DQM. Mech. Based Des. Struct. Mach. (2019). https://doi.org/10.1080/15397734.2019.1646137
40. A. Alibeigloo, A.R.P. Noee, Static and free vibration analysis of sandwich cylindrical shell based on theory of elasticity and using DQM. Acta Mech. **228**, 4123–4140 (2017)
41. H. Salehipour, D. Shahgholian-Ghahfarokhi, A. Shahsavar, O. Civalek, M. Edalati, Static deflection and free vibration analysis of functionally graded and porous cylindrical micro/nano shells based on the three-dimensional elasticity and modified couple stress theories. Mech. Based Des. Struct. Mach. (2020). https://doi.org/10.1080/15397734.2020.1775095
42. A.A. Parand, A. Alibeigloo, Static and vibration analysis of sandwich cylindrical shell with functionally graded core and viscoelastic interface using DQM. Compos. B Eng. **126**, 1–16 (2017)
43. A. Alibeigloo, Three dimensional coupled thermoelasticity solution of sandwich plate with FGM core under thermal shock. Compos. Struct. **177**, 96–103 (2017)
44. V.N. Van Do, C.-H. Lee, Static bending and free vibration analysis of multilayered composite cylindrical and spherical panels reinforced with graphene platelets by using isogeometric analysis method. Eng. Struct. **215**, 110682 (2020)
45. M.A. Biot, Theory of buckling of a porous slab and its thermoelastic analogy. J. Appl. Mech. DOI **10**(1115/1), 3629586 (1964)
46. M.A. Biot, Consolidation settlement under a rectangular load distribution. J. Appl. Phys. **12**, 426–430 (1941)
47. A.B. Rad, M. Shariyat, Three-dimensional magneto-elastic analysis of asymmetric variable thickness porous FGM circular plates with non-uniform tractions and Kerr elastic foundations. Compos. Struct. **125**, 558–574 (2015)
48. M. Sui, C. Li, W. Wu, M. Yang, H.M. Ali, Y. Zhang et al., Temperature of Grinding Carbide With Castor Oil-Based MoS2 Nanofluid Minimum Quantity Lubrication. J. Thermal Sci. Eng. Appl. **13**, 051001 (2021)
49. Z. Duan, Q. Yin, C. Li, L. Dong, X. Bai, Y. Zhang et al., Milling force and surface morphology of 45 steel under different Al_2O_3 nanofluid concentrations. Int. J. Adv. Manuf. Technol. **107**, 1277–1296 (2020)
50. T. Gao, C. Li, Y. Zhang, M. Yang, D. Jia, T. Jin et al., Dispersing mechanism and tribological performance of vegetable oil-based CNT nanofluids with different surfactants. Tribol. Int. **131**, 51–63 (2019)
51. Y. Zhang, C. Li, D. Jia, D. Zhang, X. Zhang, Experimental evaluation of the lubrication performance of MoS2/CNT nanofluid for minimal quantity lubrication in Ni-based alloy grinding. Int. J. Mach. Tools Manuf **99**, 19–33 (2015)
52. Y. Yang, H. Chen, X. Zou, X.-L. Shi, W.-D. Liu, L. Feng et al., Flexible carbon-fiber/semimetal Bi nanosheet arrays as separable and recyclable plasmonic photocatalysts and photoelectrocatalysts. ACS Appl. Mater. Interfaces. **12**, 24845–24854 (2020)
53. E. Thostenson, W. Li, D. Wang, Z. Ren, T. Chou, Carbon nanotube/carbon fiber hybrid multiscale composites. J. Appl. Phys. **91**, 6034–6037 (2002)
54. H.-S. Shen, A comparison of buckling and postbuckling behavior of FGM plates with piezoelectric fiber reinforced composite actuators. Compos. Struct. **91**, 375–384 (2009)
55. M. Rafiee, X. Liu, X. He, S. Kitipornchai, Geometrically nonlinear free vibration of shear deformable piezoelectric carbon nanotube/fiber/polymer multiscale laminated composite plates. J. Sound Vib. **333**, 3236–3251 (2014)
56. M. Kim, Y.-B. Park, O.I. Okoli, C. Zhang, Processing, characterization, and modeling of carbon nanotube-reinforced multiscale composites. Compos. Sci. Technol. **69**, 335–342 (2009)
57. M. Rafiee, J. Yang, S. Kitipornchai, Large amplitude vibration of carbon nanotube reinforced functionally graded composite beams with piezoelectric layers. Compos. Struct. **96**, 716–725 (2013)
58. H. Wu, S. Kitipornchai, J. Yang, Imperfection sensitivity of thermal post-buckling behaviour of functionally graded carbon nanotube-reinforced composite beams. Appl. Math. Model. **42**, 735–752 (2017)
59. F. Ebrahimi, A. Dabbagh, Vibration analysis of multi-scale hybrid nanocomposite plates based on a Halpin-Tsai homogenization model. Compos. Part B Eng. **173**, 106955 (2019)
60. M.H. Sadd, *Elasticity: Theory, Applications, and Numerics* (Academic Press, 2009)

61. J.N. Reddy, *Mechanics of Laminated Composite Plates and Shells: Theory and Analysis* (CRC Press, 2003)
62. B. Mou, X. Li, Y. Bai, L. Wang, Shear behavior of panel zones in steel beam-to-column connections with unequal depth of outer annular stiffener. J. Struct. Eng. **145**, 04018247 (2019)
63. N. Gao, X. Guo, J. Deng, B. Cheng, H. Hou, Elastic wave modulation of double-leaf ABH beam embedded mass oscillator. Appl. Acoust. **173**, 107694 (2021)
64. X. Zhao, B. Chen, Y. Li, W. Zhu, F. Nkiegaing, Y. Shao, Forced vibration analysis of Timoshenko double-beam system under compressive axial load by means of Green's functions. J. Sound Vib. **464**, 115001 (2020)
65. X. Zhao, W. Zhu, Y. Li, Analytical solutions of nonlocal coupled thermoelastic forced vibrations of micro-/nano-beams by means of Green's functions. J. Sound Vib. **481**, 115407 (2020)
66. M. Ye, J. Jiang, H. Chen, H. Zhou, D. Song, Seismic behavior of an innovative hybrid beam-column connection for precast concrete structures. Eng. Struct. **227**, 111436 (2021)
67. M. Sun, L. Yan, L. Zhang, L. Song, J. Guo, H. Zhang, New insights into the rapid formation of initial membrane fouling after in-situ cleaning in a membrane bioreactor. Process Biochem. **78**, 108–113 (2019)
68. G. Cederbaum, L. Li, K. Schulgasser, *Poroelastic Structures* (Elsevier, 2000)
69. C. Shu, *Differential Quadrature and Its Application in Engineering* (Springer, 2012)
70. M. Al-Furjan, S.Y. Bolandi, M. Habibi, F. Ebrahimi, G. Chen, H. Safarpour, Enhancing vibration performance of a spinning smart nanocomposite reinforced microstructure conveying fluid flow. Eng. Comput. (2021). https://doi.org/10.1007/s00366-020-01255-w
71. M. Al-Furjan, R. Dehini, M. Paknahad, M. Habibi, H. Safarpour, On the nonlinear dynamics of the multi-scale hybrid nanocomposite-reinforced annular plate under hygro-thermal environment. Arch. Civ. Mech. Eng. **21**, 1–25 (2021)
72. H. Liu, S. Shen, K. Oslub, M. Habibi, H. Safarpour, Amplitude motion and frequency simulation of a composite viscoelastic microsystem within modified couple stress elasticity. Eng. Comput. (2021). https://doi.org/10.1007/s00366-021-01316-8
73. M. Al-Furjan, M. Habibi, D.W. Jung, G. Chen, M. Safarpour, H. Safarpour, Chaotic responses and nonlinear dynamics of the graphene nanoplatelets reinforced doubly-curved panel. Eur. J. Mech. -A/Solids **85**, 104091 (2020)
74. M. Al-Furjan, M.A. Oyarhossein, M. Habibi, H. Safarpour, D.W. Jung, Frequency and critical angular velocity characteristics of rotary laminated cantilever microdisk via two-dimensional analysis. Thin-Walled Struct. **157**, 107111 (2020)
75. M. Al-Furjan, M. Habibi, D.W. Jung, H. Safarpour, M. Safarpour, On the buckling of the polymer-CNT-fiber nanocomposite annular system under thermo-mechanical loads. Mech. Based Des. Struct. Mach. (2020). https://doi.org/10.1080/15397734.2020.1830106
76. M. Al-Furjan, M. Habibi, F. Ebrahimi, G. Chen, M. Safarpour, H. Safarpour, A coupled thermomechanics approach for frequency information of electrically composite microshell using heat-transfer continuum problem. Eur. Phys. J. Plus **135**, 1–45 (2020)
77. M. Al-Furjan, M. Habibi, H. Safarpour, Vibration control of a smart shell reinforced by graphene nanoplatelets. Int. J. Appl. Mech. **12**, 2050066 (2020)
78. M. Habibi, M. Safarpour, H. Safarpour, Vibrational characteristics of a FG-GPLRC viscoelastic thick annular plate using fourth-order Runge-Kutta and GDQ methods. Mech. Based Des. Struct. Mach. (2020). https://doi.org/10.1080/15397734.2020.1779086
79. A. Shariati, M. Habibi, A. Tounsi, H. Safarpour, and M. Safa, Application of exact continuum size-dependent theory for stability and frequency analysis of a curved cantilevered microtubule by considering viscoelastic properties. Eng. Comput. (2020)
80. C. Shu, B.E. Richards, Application of generalized differential quadrature to solve two-dimensional incompressible Navier-Stokes equations. Int. J. Numer. Meth. Fluids **15**, 791–798 (1992)
81. M. Karimiasl, F. Ebrahimi, B. Akgöz, "Buckling and post-buckling responses of smart doubly curved composite shallow shells embedded in SMA fiber under hygro-thermal loading. Compos. Struct. **223**, 110988 (2019)
82. M. Jabbari, S. Karampour, M. Eslami, Steady state thermal and mechanical stresses of a poro-piezo-FGM hollow sphere. Meccanica **48**, 699–719 (2013)
83. J. Reddy, C. Wang, S. Kitipornchai, Axisymmetric bending of functionally graded circular and annular plates. Eur. J. Mech. A/Solids **18**, 185–199 (1999)
84. M. Ahmadi, R. Ansari, H. Rouhi, Multi-scale bending, buckling and vibration analyses of carbon fiber/carbon nanotube-reinforced polymer nanocomposite plates with various shapes. Phys. E. **93**, 17–25 (2017)